MODIFICATIONS TO A TWO-CONTROL-VOLUME, FREQUENCY DEPENDENT,

TRANSFER-FUNCTION ANALYSIS OF HOLE-PATTERN GAS ANNULAR SEALS

A Thesis

by

YOON SHIK SHIN

Submitted to the Office of Graduate Studies of
Texas A&M University
in partial fulfillment of the requirements for the degree of

MASTER OF SCIENCE

December 2005

Major Subject: Mechanical Engineering

MODIFICATIONS TO A TWO-CONTROL-VOLUME, FREQUENCY DEPENDENT,

TRANSFER-FUNCTION ANALYSIS OF HOLE-PATTERN GAS ANNULAR SEALS

A Thesis

by

YOON SHIK SHIN

Submitted to the Office of Graduate Studies of
Texas A&M University
in partial fulfillment of the requirements for the degree of

MASTER OF SCIENCE

Approved by:

Chair of Committee,   Dara W. Childs
Committee Members, Gerald L. Morrison
                                 Yassin A. Hassan
Head of Department,   Dennis O'Neal

December 2005

Major Subject: Mechanical Engineering

ABSTRACT

Modifications to a Two-Control-Volume, Frequency Dependent, Transfer-Function
Analysis of Hole-Pattern Gas Annular Seals. (December 2005)

Yoon Shik Shin, B.S., Yonsei University

Chair of Advisory Committee: Dr. Dara W. Childs

A rotordynamic analysis of hole-pattern gas annular seals using a two-control-volume model, Ha and Childs and frequency dependent transfer-function model, Kleynhans and Childs is modified with four features. The energy equation is added, and real gas properties are used instead of the ideal gas equation of state. The depth of the hole-pattern is made variable with the axial distance along the seal. And last, the addition of deep grooves to hole-pattern seals is analyzed, and the code's predictions for the influence of a groove are compared with test data.

DEDICATION

To my wife, Seung-Yeon

TABLE OF CONTENTS

LIST OF FIGURES

LIST OF TABLES

NOMENCLATURE

Roman

C, c	Direct and cross-coupled damping coefficient, [FT/L]
C_{eff}	Effective damping coefficient introduced in Eq. (31), [FT/L]
C_r	Seal radial clearance, [L]
c_r	Non-dimensional seal radial clearance introduced in Eq. (A7), [-]
C_v	Specific heat at constant volume, $[L^2/(T^2\Theta)]$
D	Seal diameter, [L]
$\boldsymbol{D}$	Direct force impedance due to displacement, [F/L]
$\boldsymbol{D}_{\varepsilon\alpha}$	Direct force impedance due to tilting, [F]
$\boldsymbol{D}_{\alpha\varepsilon}$	Direct moment impedance due to displacement, [F]
$\boldsymbol{D}_{\alpha}$	Direct moment impedance due to tilting, [FL]
e	Internal energy introduced in Eq. (12), $[L^2/T^2]$
$\boldsymbol{E}$	Cross-coupled force impedance due to displacement, [F/L]
$\boldsymbol{E}_{\varepsilon\alpha}$	Cross-coupled force impedance due to tilting, [F]
$\boldsymbol{E}_{\alpha\varepsilon}$	Cross-coupled moment impedance due to displacement, [F]
$\boldsymbol{E}_{\alpha}$	Cross-coupled moment impedance due to tilting, [FL]
f	Non-dimensional frequency introduced in Eq. (A78), [-]
f_s, f_r	Friction factor of stator and rotor introduced in Eqs. (20)-(21), [-]
F_X, F_Y	Components of seal reaction force introduced in Eqs. (A97)-(A98), [F]
$\tilde{F}_X, \tilde{F}_Y$	Non-dimensional components of seal reaction force introduced in Eqs. (A93)-(A94), [-]
H	Local clearance [L]
h	Non-dimensional local clearance introduced in Eq. (A5), [-]
H_d	Hole depth, [L]
h_d	Non-dimensional hole depth introduced in Eq. (A6), [-]
j	$\sqrt{-1}$
K, k	Direct and cross-coupled stiffness coefficient, [F/L]

K_{eff}	Effective stiffness coefficient introduced in Eq. (30), [F/L]
L	Seal length, [L]
l	Non-dimensional seal length introduced in Eq. (A8), [-]
M	Direct added mass coefficient, [M]
M_X, M_Y	Components of seal reaction moment introduced in Eqs. (A99)-(A100), [FL]
$\tilde{M}_X$, $\tilde{M}_Y$	Non-dimensional components of seal reaction moment introduced in Eqs. (A95)-(A96), [-]
Ma	Mach number, [-]
n	Blasius friction factor coefficient, [-]
m	Blasius friction factor exponent, [-]
$\dot{m}$	Mass flow rate, [M/T]
$\dot{\tilde{m}}$	Non-dimensional mass flow rate introduced in Eq. (A50), [-]
P	Pressure, [F/L^2]
p	Non-dimensional pressure introduced in Eq. (A2), [-]
P_c	Pressure coefficient introduced in Eq. (A19), [-]
R	Seal radius, [L]
Re	Reynolds number, [-]
T	Temperature, [Θ]
t	Time, [T]
U	Circumferential bulk fluid velocity, [L/T]
u	Non-dimensional circumferential bulk fluid velocity introduced in Eq. (A3), [-]
$\hat{u}$	Internal energy introduced in Eq. (13), [L^2/T^2]
$\tilde{\hat{u}}$	Non-dimensional internal energy introduced in Eq. (A12), [-]
$\hat{u}_c$	Internal energy coefficient introduced in Eq. (A20), [-]
V	Radial bulk fluid velocity, [L/T]
$\forall$	Volume, [L^3]

W	Axial bulk fluid velocity, [L/T]
w	Non-dimensional axial bulk fluid velocity introduced in Eq. (A1), [-]
X, Y	Relative displacement between stator and rotor, [L]
x, y	Non-dimensional relative displacement between stator and rotor, [-]
Z	Axial coordinate, [L]
z	Non-dimensional axial coordinate introduced in Eq. (A9), [-]
z_0	Non-dimensional center-position of tilting motion, [-]
Z_c	Compressibility factor, [-]

Greek

α_X, α_Y	Relative seal rotations about transverse X, Y axes, [-]
γ	Specific heat ratio, [-]
γ_c	Ratio of hole-pattern area to total stator surface area, [-]
ε	Perturbation eccentricity ratio, [-]
κ	Viscosity power law exponent, [-]
μ	Fluid viscosity, [FT/L^2]
ρ	Fluid density, [M/L^3]
$\tilde{\rho}$	Non-dimensional fluid density introduced in Eq. (A4), [-]
τ	Non-dimensional time introduced in Eq. (A10), [-]
$\tau_{sz}, \tau_{rz}, \tau_{s\theta}, \tau_{r\theta}$	Shear stress introduced in Eqs. (14)-(17), [F/L^2]
Ω	Rotor precessional frequency, [1/T]
Φ	Flow coefficient introduced in Eq. (33), [-]
ω	Rotor rotational frequency, [1/T]

Subscripts

in, ex	Inlet and exit, respectively
R, S	Denotes reservoir and sump, respectively
r, s	Denotes rotor and stator, respectively
z, θ	Axial and circumferential, respectively

α	Moment component due to tilting motion
αε	Moment component due to displacement motion
εα	Force component due to tilting motion
0, 1	Zeroth-order and first-order perturbations in the dependent variables, respectively

1. INTRODUCTION

The function of annular seal is leakage control between different pressure regions in turbomachinery. Figure 1 shows a hole-pattern seal and a smooth rotor. Seals can also affect rotordynamic performance significantly. Historically, labyrinth seals are used widely because of lower cost and good leakage control. However, labyrinth seals have relatively low effective damping which can cause instability in high performance turbomachinery. Childs and Moyer [1] discussed the replacement of labyrinth seals with honeycomb seals in the HPOTP (High Pressure Oxygen Turbopump) of the SSME (Space Shuttle Main Engine) to resolve synchronous and subsynchronous vibration problems. Recently, hole-pattern seals are more widely used because of close performance to honeycomb seals and even lower cost, Yu and Childs [2].
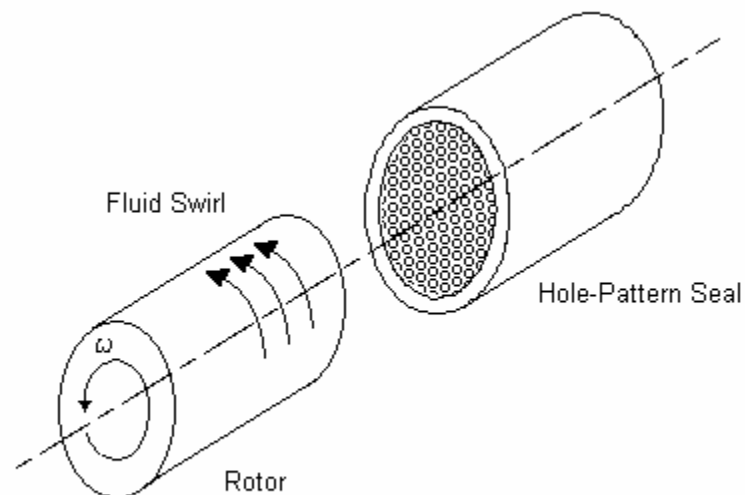
Figure 1 Hole-pattern seal and rotor

_____

This thesis follows the style of the ASME Journal of Tribology.

A full analysis of gas annular seal is first presented by Nelson [3], [4]. Nelson's bulk flow, one-control-volume model gave reasonable predictions for smooth stator/smooth rotor seals. However, for honeycomb stator/smooth rotor seals, the honeycomb surface was regarded as a 'rough surface', and the prediction was poor. The two-control-volume model is provided by Ha and Childs [5], but no solution is given. Kleynhans and Childs [6] introduced frequency dependent, transfer-function model, because the traditional force/motion relationship of Eq. (1) is not valid for two-control-volume analysis results.

$$-\begin{Bmatrix} F_X \\ F_Y \end{Bmatrix} = \begin{bmatrix} K & k \\ -k & K \end{bmatrix} \begin{Bmatrix} X \\ Y \end{Bmatrix} + \begin{bmatrix} C & c \\ -c & C \end{bmatrix} \begin{Bmatrix} \dot{X} \\ \dot{Y} \end{Bmatrix} + M \begin{Bmatrix} \ddot{X} \\ \ddot{Y} \end{Bmatrix} \qquad (1)$$

Kleynhans and Childs [6] developed a solution code using two-control-volume, constant temperature model that produced a frequency dependent, transfer-function model. The solution showed a very good match with test results by Childs and Wade [7].

2. OBJECTIVES

This study starts from the following questions:

(a) Comparing to the isothermal model of Kleynhans and Childs [6], how do property changes due to temperature distribution affect the zeroth and first order perturbation solutions?

(b) For high-pressure gas mixtures, how large is the difference between an ideal gas solution and a solution with real gas properties?

(c) If a hole-pattern seal has varying hole-depth along the axial direction, would it improve any performance features of the seal? What kind of hole-depth axial variation is ideal?

(d) Considering a hole-pattern seal with a deep annular groove somewhere along the surface, what is the best location for the groove? How are characteristics of gas annular seal affected by a deep annular groove?

3. GOVERNING EQUATIONS

The governing equations start from those presented by Ha and Childs [5]. Figure 2 shows the location of control volumes. Note that the clearance is exaggerated for clarity.
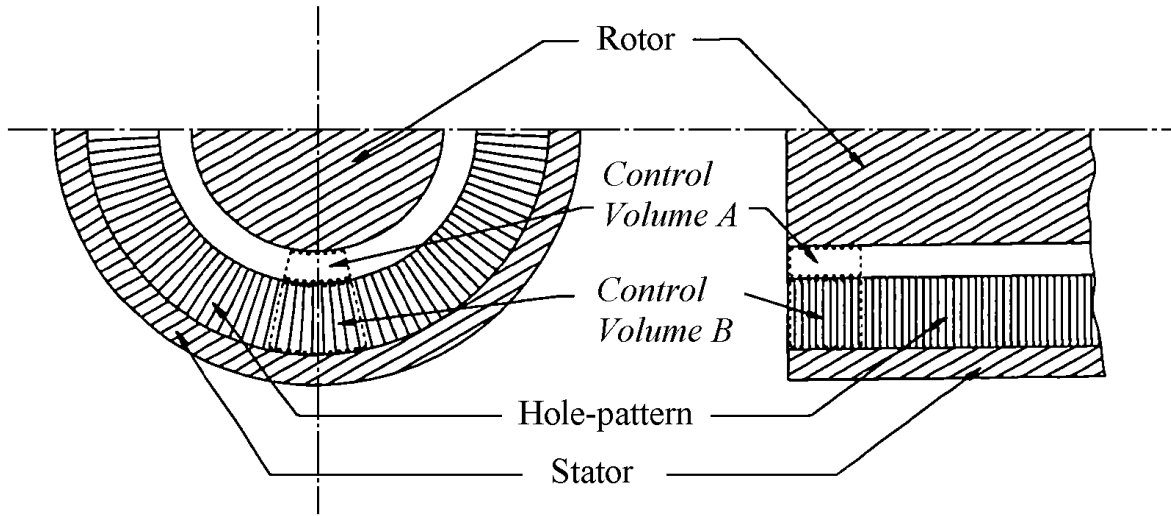
Figure 2 Cross-sectional view of hole-pattern seal/smooth rotor

The integral forms of bulk-flow governing equations are:

Continuity

$$0 = \frac{\partial}{\partial t} \oint_{C\forall} \rho \, d\forall + \oint_{CS} \rho \vec{v} \cdot d\vec{A} \tag{2}$$

Axial Momentum

$$\sum F_Z = \frac{\partial}{\partial t} \oint_{C\forall} \rho W \, d\forall + \oint_{CS} \rho W \vec{v} \cdot d\vec{A} \tag{3}$$

Circumferential Momentum

$$\sum F_\theta = \frac{\partial}{\partial t} \oint_{C\forall} \rho U \, d\forall + \oint_{CS} \rho U \vec{v} \cdot d\vec{A} \tag{4}$$

Energy

$$-\dot{W}_v = \frac{\partial}{\partial t}\oint_{CV}e\rho d\forall + \oint_{CS}\left(e+\frac{P}{\rho}\right)\rho\vec{v}\cdot d\vec{A}.$$ (5)

The flows shown in Figure 3 are expressed in differential forms:
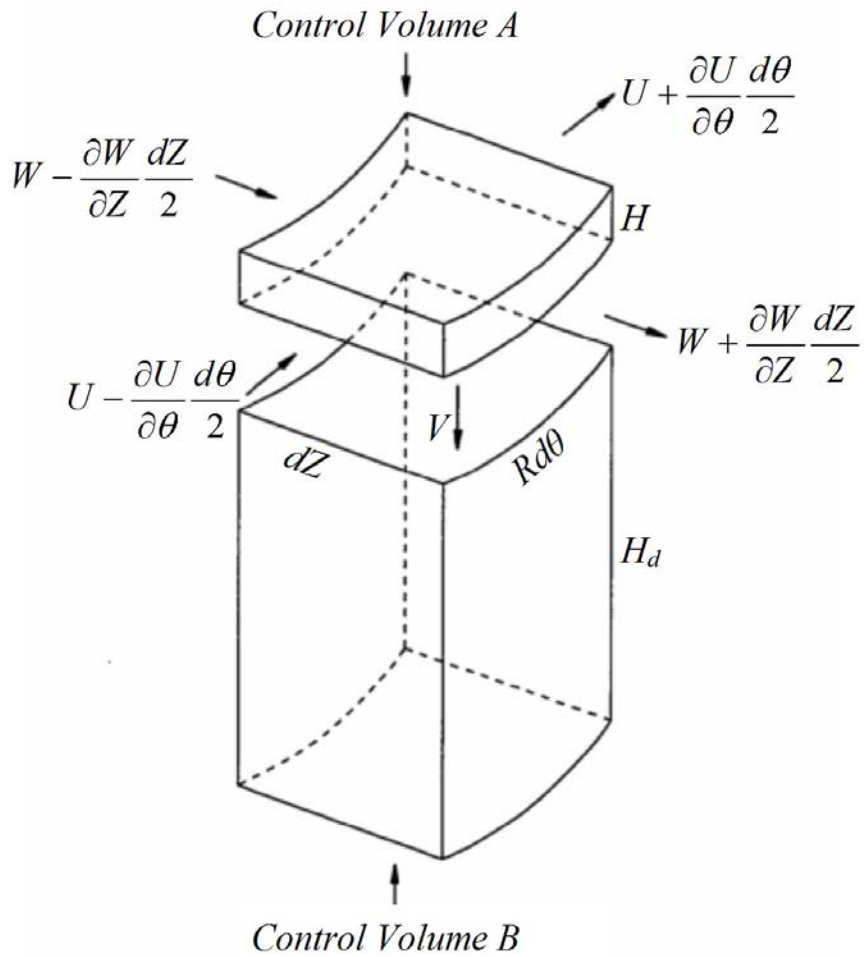
Figure 3 Flow in and out through control volume surface

Continuity Equation for control volume A

$$\frac{\partial}{\partial t}(\rho H) + \frac{1}{R}\frac{\partial}{\partial \theta}(\rho UH) + \frac{\partial}{\partial Z}(\rho WH) + \rho V = 0 \tag{6}$$

Continuity Equation for control volume B

$$\rho V = \gamma_c H_d \frac{\partial \rho}{\partial t} \tag{7}$$

Axial momentum equation

$$-H\frac{\partial P}{\partial Z} = \tau_{sz} + \tau_{rz} + \rho WV + \frac{\partial(\rho HW)}{\partial t} + \frac{\partial(\rho HWU)}{R\partial \theta} + \frac{\partial(\rho HW^2)}{\partial Z} \tag{8}$$

Circumferential momentum equation

$$-\frac{H}{R}\frac{\partial P}{\partial \theta} = \tau_{s\theta} + \tau_{r\theta} + \rho UV + \frac{\partial(\rho HU)}{\partial t} + \frac{\partial(\rho HU^2)}{R\partial \theta} + \frac{\partial(\rho HWU)}{\partial Z} \tag{9}$$

Energy equation

$$0 = \rho H\frac{De}{Dt} + \rho\gamma_c H_d\frac{\partial e}{\partial t} + \frac{\partial}{\partial Z}(PWH) + \frac{1}{R}\frac{\partial}{\partial \theta}(PUH) + R\omega\tau_{r\theta} \tag{10}$$

where,

$$\frac{D}{Dt} = \frac{\partial}{\partial t} + \frac{U}{R}\frac{\partial}{\partial \theta} + W\frac{\partial}{\partial Z} \tag{11}$$

$$e = \hat{u} + \frac{U^2}{2} + \frac{W^2}{2} \tag{12}$$

$$\hat{u} = C_v T = \frac{1}{Z_c(\gamma-1)}\frac{P}{\rho}. \tag{13}$$

The variable *V*, transient radial velocity from *Control Volume A* to *Control Volume B*, can be eliminated by substituting *V* from Eq. (7) into Eqs. (6), (8) and (9).

For the analysis using general real gas properties, the internal energy $\hat{u}$ and its partial derivatives are directly obtained with the code by Huber [8] (NIST SUPERTRAPP) instead of ideal gas relationship. Following the analyses of Nelson [3], [4] and Ha and Childs [5], the energy balance is modeled as adiabatic flow; therefore, no heat flow rate term appears in the energy equation.

The hole-depth H_d appearing in Eq. (7) was treated as constant in prior analyses, but in Section 6 of this thesis, H_d is considered to vary with axial position in the seal. Accordingly, H_d is function of Z. The functions for $H_d(Z)$ are specified in Section 6.

Shear stresses are expressed as:

$$\tau_{sz} = \frac{1}{2} \rho W U_s f_s \tag{14}$$

$$\tau_{rz} = \frac{1}{2} \rho W U_r f_r \tag{15}$$

$$\tau_{s\theta} = \frac{1}{2} \rho U U_s f_s \tag{16}$$

$$\tau_{r\theta} = \frac{1}{2} \rho (U - R\omega) U_r f_r \tag{17}$$

where,

$$U_s = \sqrt{W^2 + U^2} \tag{18}$$

$$U_r = \sqrt{W^2 + (U - R\omega)^2} . \tag{19}$$

D'Souza and Childs [9] compared various friction factor models and concluded that the Blasius' model showed good result with the following relatively simple formulas.

$$f_s = n_s \left(\frac{2\rho U_s H}{\mu} \right)^{m_s} \tag{20}$$

$$f_r = n_r \left(\frac{2\rho U_r H}{\mu} \right)^{m_r} \tag{21}$$

Temperature dependent viscosity, μ is directly obtained from NIST SUPERTRAPP code. The viscosity also can be calculated with a common approximation of Eq. (22).

$$\frac{\mu}{\mu_R} = \left(\frac{T}{T_R} \right)^{\kappa} \tag{22}$$

where, κ is fluid's own constant. For air, $\kappa = 0.7$.

The sudden contraction with loss at the inlet is modeled as

$$P_R - P(0) = \frac{1 + \xi}{2} \rho(0) W^2(0) , \tag{23}$$

and an ideal gas isentropic relationship is used between just before and just after the inlet.

$$\frac{P(0)}{P_R} = \left(\frac{\rho(0)}{\rho_R}\right)^{\gamma} \tag{24}$$

Exit recovery is modeled as

$$P_S - P(1) = \frac{1-\xi_e}{2}\rho(1)W^2(1). \tag{25}$$

Nelson [3], [4] introduced a gas-dynamic model of Mach number dependent inlet loss boundary conditions for pressure and density, instead of Eqs. (23) and (24). Since, Nelson's model showed even less realistic results, Kleynhans and Childs [6] used simple approximations as Eqs. (23) and (25) which is based on liquid seal model, and showed good predictions.

The solution procedure of zeroth and first order perturbation governing equation is given in Appendix A. The solution in Appendices is extended to force and moment coefficients due to displacement and tilting motion. Once the solution is obtained, the first order perturbation pressure is integrated to get perturbation reaction force. The general transfer function on two-control-volume is,

$$-\begin{Bmatrix} F_X(j\Omega) \\ F_Y(j\Omega) \end{Bmatrix} = \begin{bmatrix} D(j\Omega) & E(j\Omega) \\ -E(j\Omega) & D(j\Omega) \end{bmatrix}\begin{Bmatrix} X(j\Omega) \\ Y(j\Omega) \end{Bmatrix}, \tag{26}$$

where, Ω is rotor precession frequency, $F_X(j\Omega)$ and $F_Y(j\Omega)$ are reaction force vector components, and $X(j\Omega)$, $Y(j\Omega)$ are the components of the relative displacement vector between stator and rotor. In terms of frequency dependent rotordynamic coefficients, the model is,

$$-\begin{Bmatrix} F_X \\ F_Y \end{Bmatrix} = \begin{bmatrix} K(\Omega) & k(\Omega) \\ -k(\Omega) & K(\Omega) \end{bmatrix}\begin{Bmatrix} X \\ Y \end{Bmatrix} + \begin{bmatrix} C(\Omega) & c(\Omega) \\ -c(\Omega) & C(\Omega) \end{bmatrix}\begin{Bmatrix} \dot{X} \\ \dot{Y} \end{Bmatrix}. \tag{27}$$

Therefore,

$$D(j\Omega) = K(\Omega) + jC(\Omega) \tag{28}$$

$$E(j\Omega) = k(\Omega) + jc(\Omega). \tag{29}$$

The frequency dependent force effective stiffness and effective damping are calculated as following:

$$K_{eff}(\Omega) = K(\Omega) + c(\Omega)\Omega \qquad (30)$$

$$C_{eff}(\Omega) = C(\Omega) - \frac{k(\Omega)}{\Omega}. \qquad (31)$$

4. EFFECT OF THE ENERGY EQUATION

In this section, the effect of energy equation is examined by performing numerical experiment with both the new model and the isothermal model of Kleynhans and Childs [6] in the same conditions. The predictions of two models are compared with test results by Kerr and Childs [10], and Childs and Wade [7].

4.1. Static Solution

The running conditions and geometries are,

- $P_R = 70$ bars
- $P_S = 34.3$ bars
- $D = 114.74$ mm
- $L = 86.055$ mm
- $H_d = 3.3$ mm
- $\gamma_c = 0.684$
- $\mu = 1.876E-5$ Pa sec
- *Preswirl ratio* = 0.303
- *Molecular weight* = 28.96
- $\gamma = 1.4$
- $m_s = -0.1101$
- $n_s = 0.0785$
- $m_r = -0.217$
- $n_r = 0.0586.$

Pressure and density distributions along the axial direction decide the temperature distribution. Exit temperatures are predicted for adiabatic flow. The predictions of exit temperature and mass flow rate are compared in Table 1 with test results by Childs and Wade [7]. 'ISOT' represents the code developed by Kleynhans and Childs [6], with constant temperature and ideal gas equation. 'ENERGY' is the modified code that

contains the energy equation. However, real gas properties are not considered in this section. Namely, 'ENERGY' has the energy equation and the ideal gas equation of state.

Table 1 Temperature drop and leakage comparison - using default values for Blasius coefficients

C_r (mm)	ω (rpm)	Inlet T (˚C)	Exit Temperature (˚C)		$\dot{m}$ (Kg/s)		
			Test	**ENERGY**	**Test**	**ISOT**	**ENERGY**
0.1	10,200	10.34	6.13	14.88	0.197	0.165	0.140
0.1	15,200	10.08	6.70	28.42	0.190	0.162	0.133
0.1	20,200	11.87	6.20	53.72	0.175	0.161	0.124
0.2	10,200	17.44	15.18	11.70	0.436	0.448	0.409
0.2	15,200	19.94	15.68	18.93	0.429	0.444	0.400
0.2	20,200	19.06	15.71	25.70	0.409	0.437	0.389

Exit temperature and leakage predicted with new model is not very close to test data. The data are saying that the Blasius friction factor coefficients currently used for the stator are not suitable for this situation. Childs and Fayolle [11] stated that friction factor is also dependent on running speed, and clearance as well. Namely, there is no constant Blausius coefficient that can predict for various running speeds and clearances. To get better results for clearance of 0.1 mm, trial-and-error study is done using Moody's pipe friction factor chart, and some constants are found that make prediction more realistic for each model of 'ISOT' and 'ENERGY'. The predictions with new constants are compared to test data again in Table 2 (ISOT) and Table 3 (ENERGY).

Table 2 Leakage comparison using new values for Blasius coefficients (n_s = 0.035, m_s = -0.1101)

C_r (mm)	ω (rpm)	Inlet T (˚C)	$\dot{m}$ (Kg/s)	
			Test	**ISOT**
0.1	10,200	10.34	0.197	0.176
0.1	15,200	10.08	0.19	0.183
0.1	20,200	11.87	0.175	0.175

Table 3 Temperature drop and leakage comparison using new values for Blasius coefficients (n_s = 0.03, m_s = -0.1101)

C_r (mm)	ω (rpm)	Inlet T (˚C)	Exit Temperature (˚C)		$\dot{m}$ (Kg/s)	
			Test	**ENERGY**	**Test**	**ENERGY**
0.1	10,200	10.34	6.13	7.93	0.197	0.197
0.1	15,200	10.08	6.7	15.86	0.19	0.19
0.1	20,200	11.87	6.2	30.66	0.175	0.18

These choices for Blausius friction factor give better results. Further, providing running speed dependent Blausius constants will make prediction even better.

4.2. Dynamic Solution

Force coefficients with 'ISOT' and 'ENERGY' are compared for a smooth seal and a hole-pattern seals. Seal geometry is same as that of static solution above. Running conditions are:

- P_R = 70 bars
- P_S = 32 bars
- T_R = 19°C (smooth seal), 10°C (hole-pattern seal)
- ω = 10,200 rpm
- H_d = 3.3 mm (hole-pattern seal)
- C_r = 0.1 mm

- *Preswirl ratio* = 0

- m_s = -0.217 (smooth seal), -0.1101 (hole-pattern seal)

- n_s = 0.0586 (smooth seal), 0.0785 (hole-pattern seal).

The rotordynamic coefficients of direct and cross-coupled stiffness and damping ($K(f)$, $k(f)$, $C(f)$, $c(f)$) are plotted with respect to non-dimensional frequency f defined in Eq. (A78). Effective stiffness K_{eff} and effective damping C_{eff} which are defined in Eqs. (30), (31) also plotted.

4.2.1 Smooth Seal

Predictions are performed up to f = 10. The test results by Kerr and Childs [10] are available up to f = 2. The comparisons of rotordynamic coefficients are shown in Figure 4 through Figure 10.
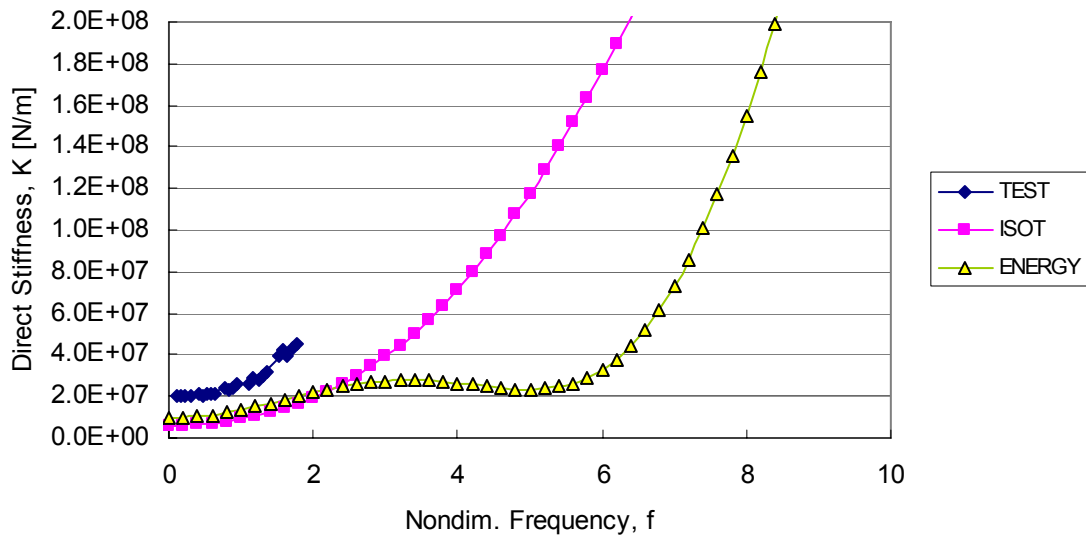
Figure 4 Direct stiffness $K(f)$ vs. non-dimensional frequency f for smooth seal

Figure 5 Cross-coupled stiffness $k(f)$ vs. non-dimensional frequency for smooth seal
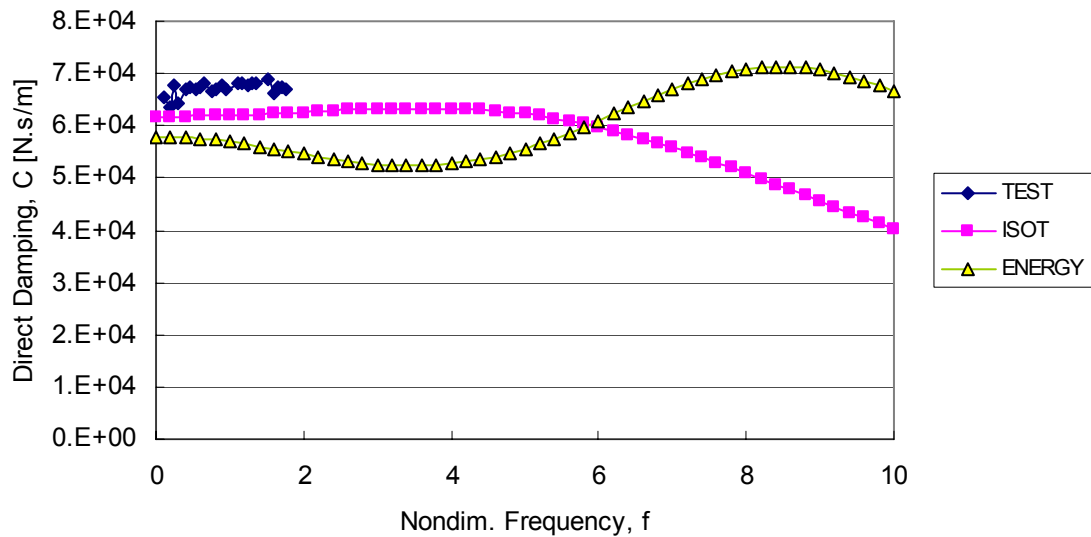
Figure 6 Direct damping $C(f)$ vs. non-dimensional frequency f for smooth seal
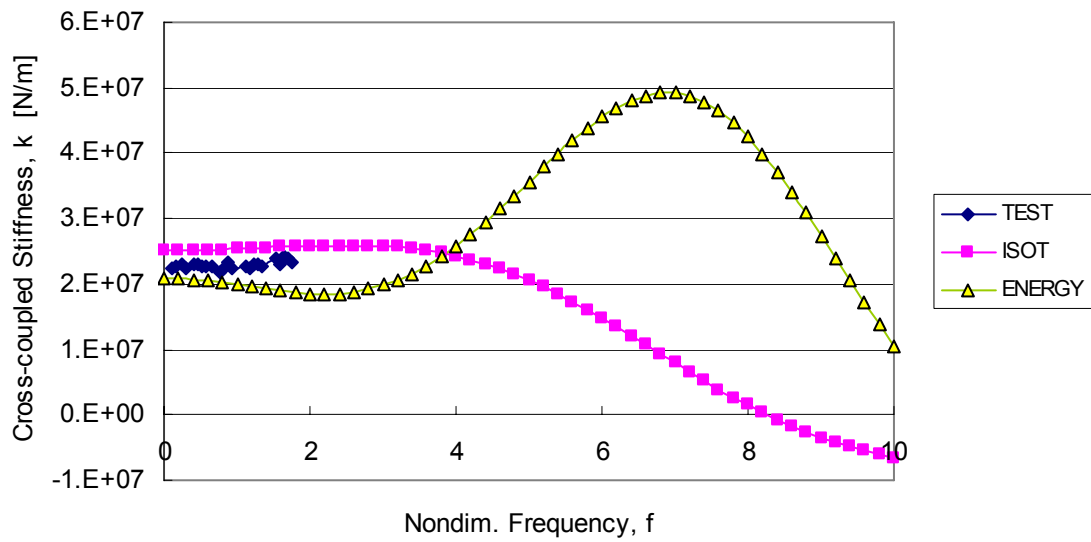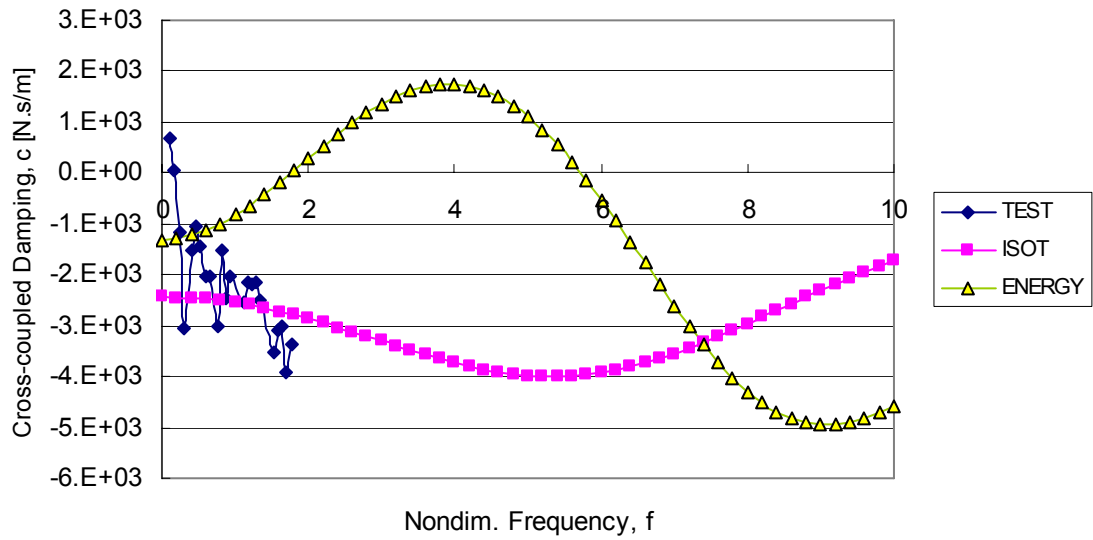
Figure 7 Cross-coupled damping $c(f)$ vs. non-dimensional frequency f for smooth seal
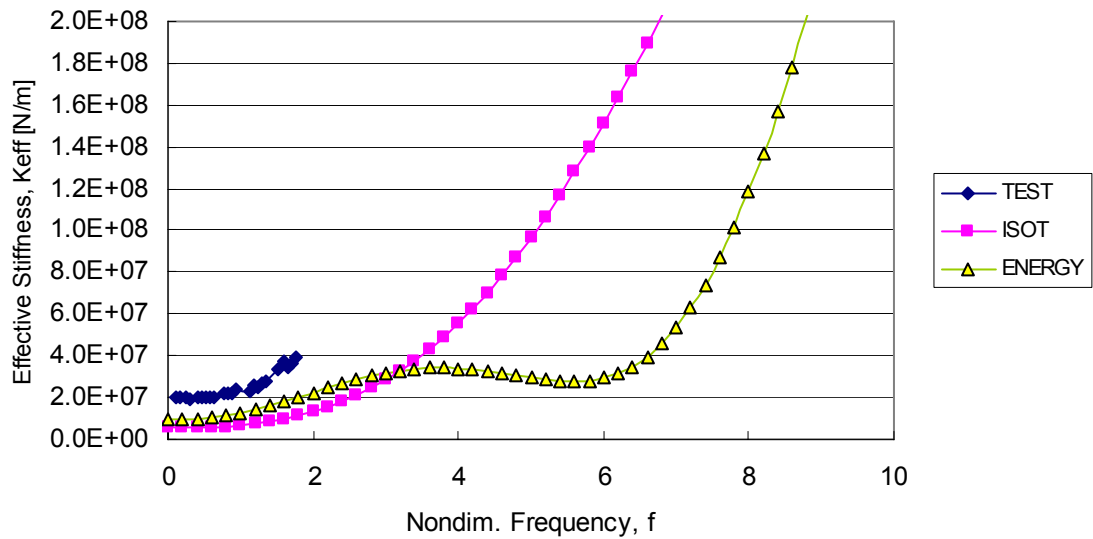
Figure 8 Effective stiffness $K_{eff}(f)$ vs. non-dimensional frequency f for smooth seal
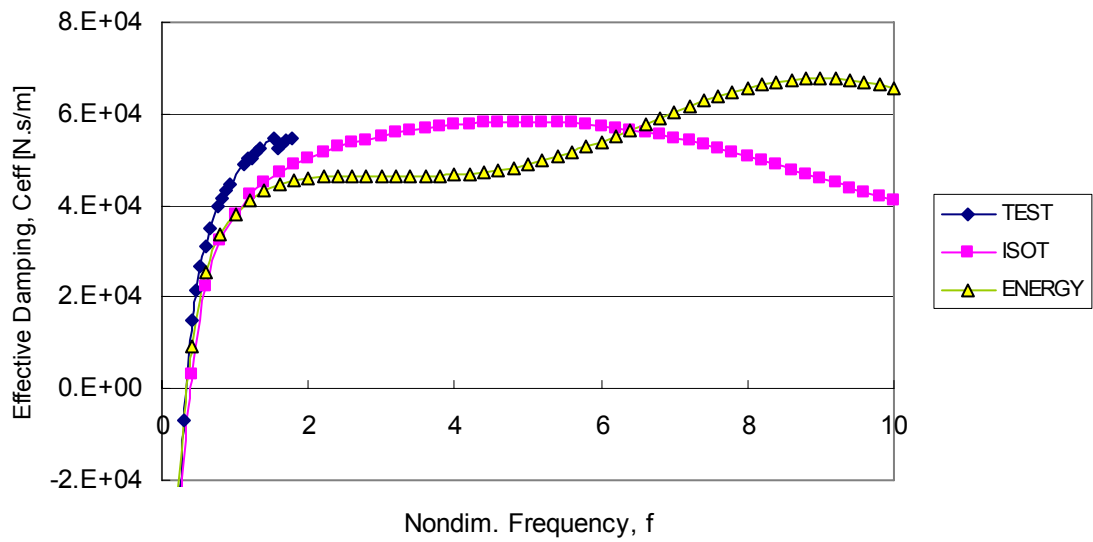
Figure 9 Effective damping $C_{eff}(f)$ vs. non-dimensional frequency f for smooth seal
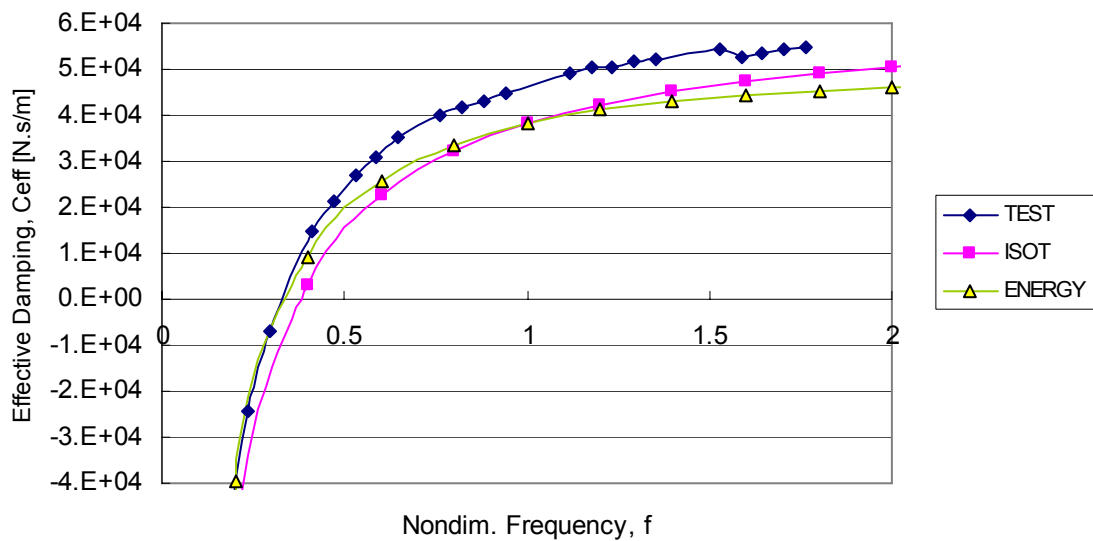
Figure 10 Effective damping $C_{eff}(f)$ vs. non-dimensional frequency f for smooth seal (detail)

For smooth seals at this condition, two models works fairly well through $0 < f < 1$. The 'ENERGY' model predicts slightly better than the 'ISOT' model. Direct stiffness is under-predicted with both models, but the 'ENERGY' model shows more realistic prediction. Effective stiffness is well predicted with the 'ENERGY' model at the non-dimensional frequency range below $f = 0.5$. At the range of $f = 1$ and higher frequencies, the 'ISOT' model shows closer prediction of effective damping to the test result. Still, the differences are very small.

4.2.2 Hole-pattern seal (h_d = 3.3mm)

The same seal as the smooth seal of the previous section now has 3.3 mm hole-pattern and is predicted with two models. In Figure 11 through Figure 22, rotordynamic coefficients are predicted and compared to test data in the same manner as the previous section. The test results are from Childs and Wade [7].

The 'ENERGY' model also shows better predictions than the 'ISOT' model for hole-pattern seals. However, differences between the two models are not significant for the non-dimensional frequency range below $f = 2$, which is the range of interest.

The difference in rotordynamic coefficients between the two models is less for hole-pattern seals than for smooth seals. This study shows that both the 'ISOT' model and the 'ENERGY' model predicts rotordynamic coefficients fairly well for the frequency range of $0 < f < 2$, and that the 'ENERGY' model gives modestly better predictions.

Figure 11 Direct stiffness $K(f)$ vs. non-dimensional frequency f for hole-pattern seal

**Figure 12 Direct stiffness $K(f)$ vs. non-dimensional frequency f for hole-pattern seal (detail)**
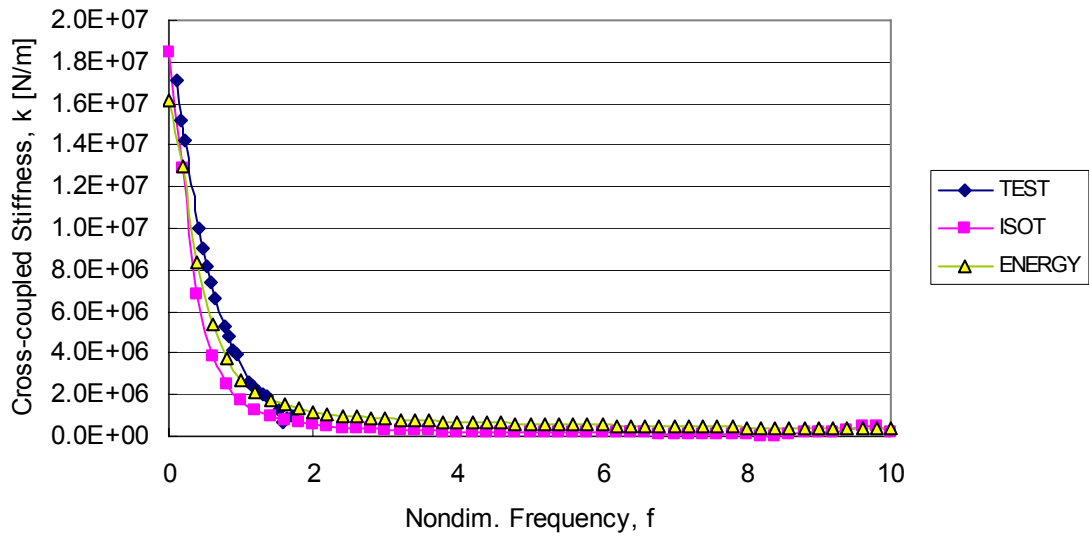
Figure 13 Cross-coupled stiffness *k*(*f*) vs. non-dimensional frequency *f* for hole-pattern seal
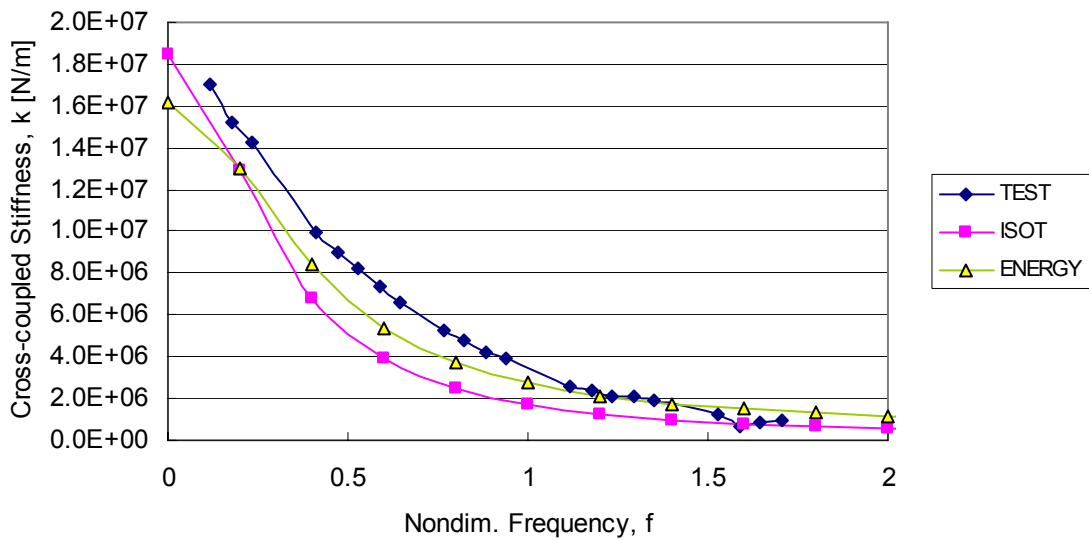
Figure 14 Cross-coupled stiffness *k*(*f*) vs. non-dimensional frequency *f* for hole-pattern seal (detail)
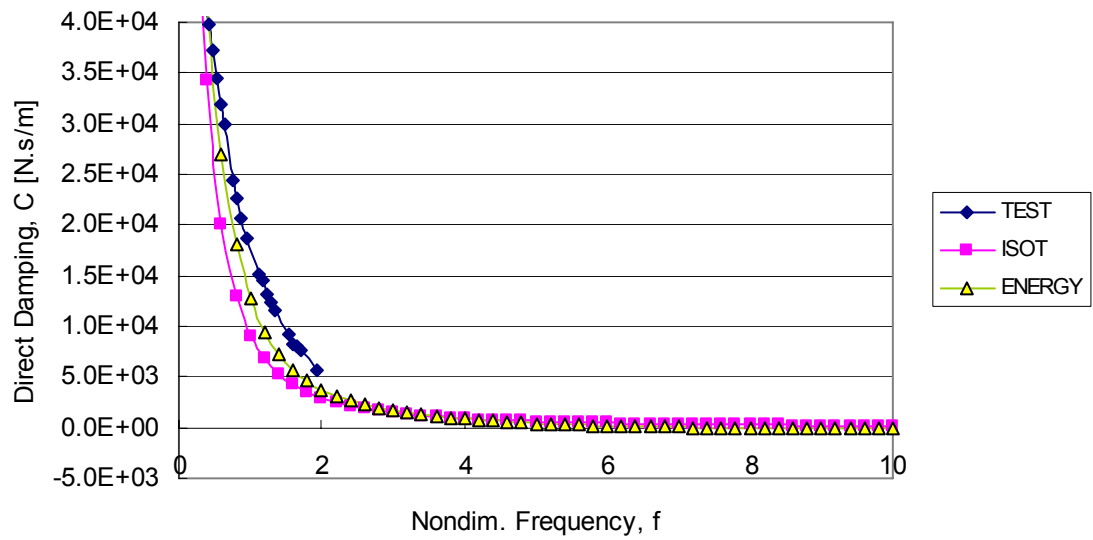
Figure 15 Direct damping *C(f)* vs. non-dimensional frequency *f* for hole-pattern seal
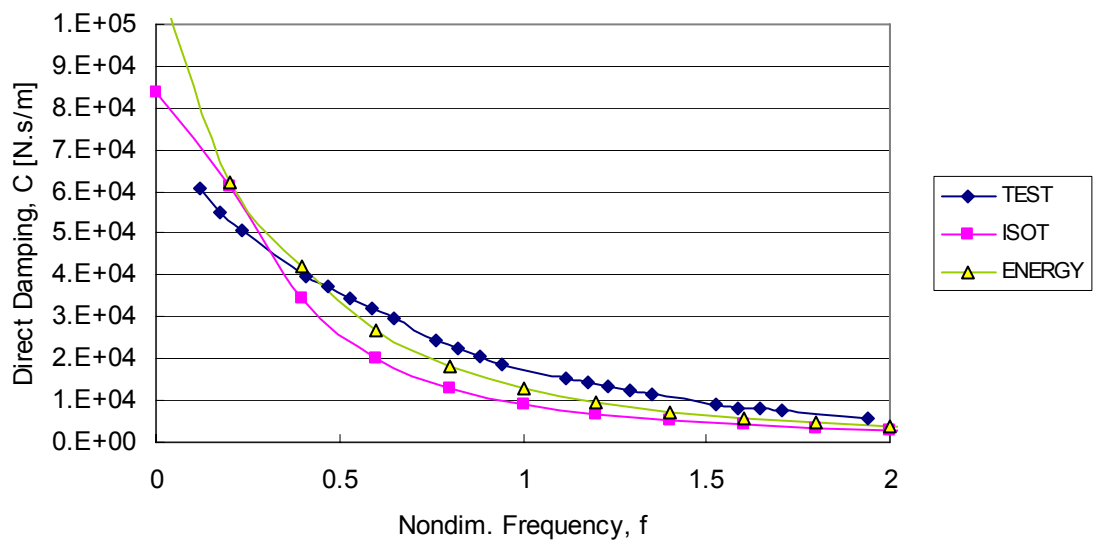
Figure 16 Direct damping *C(f)* vs. non-dimensional frequency *f* for hole-pattern seal (detail)
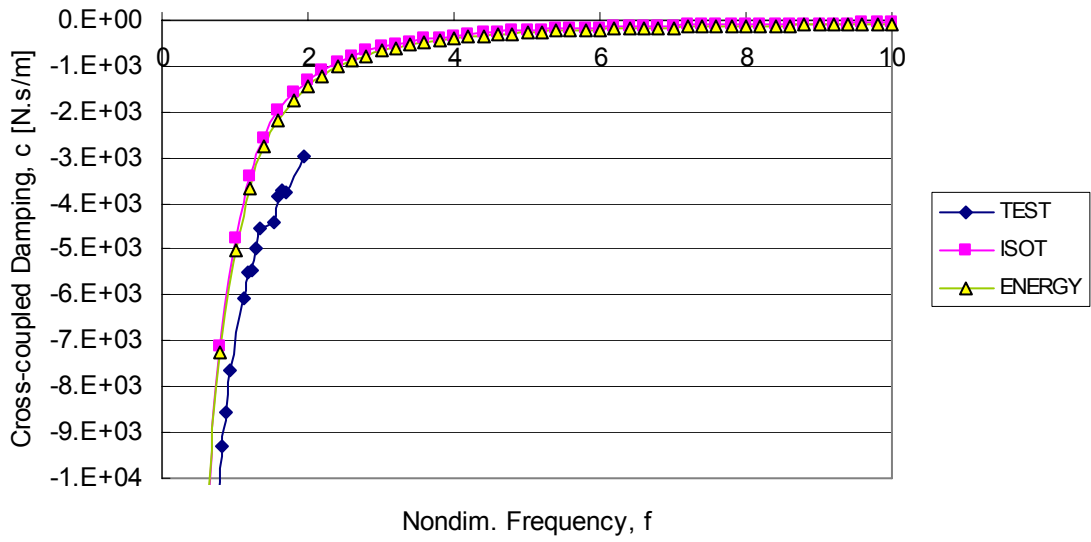
Figure 17 Cross-coupled damping *c*(*f*) vs. non-dimensional frequency *f* for hole-pattern seal
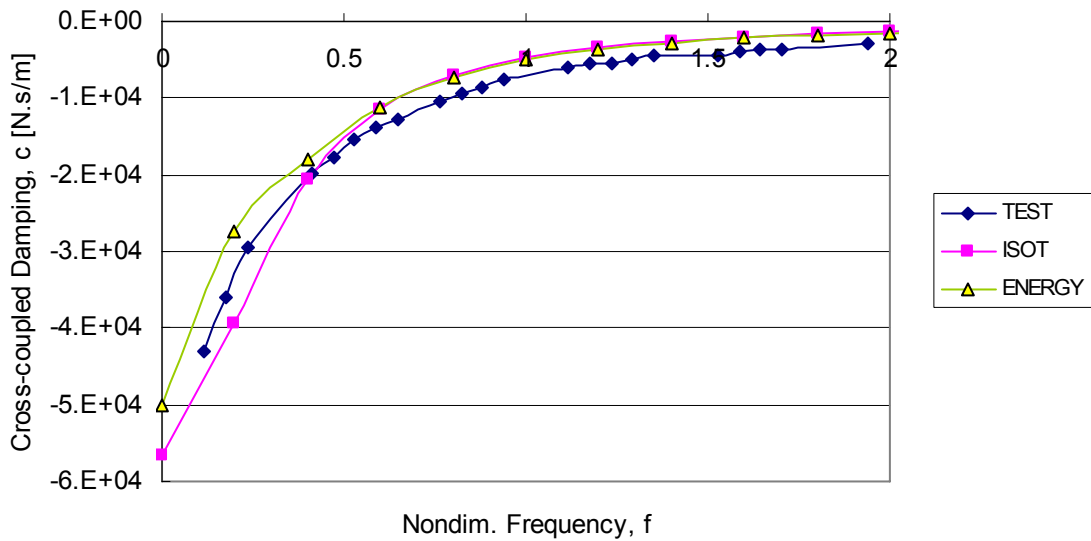
Figure 18 Cross-coupled damping *c*(*f*) vs. non-dimensional frequency *f* for hole-pattern seal (detail)
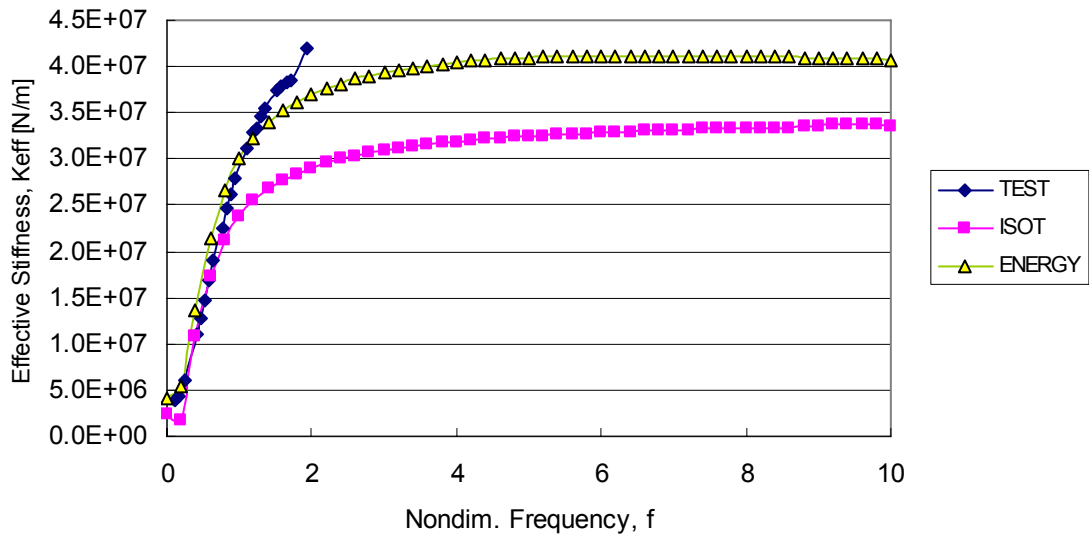
Figure 19 Effective stiffness $K_{eff}(f)$ vs. non-dimensional frequency f for hole-pattern seal

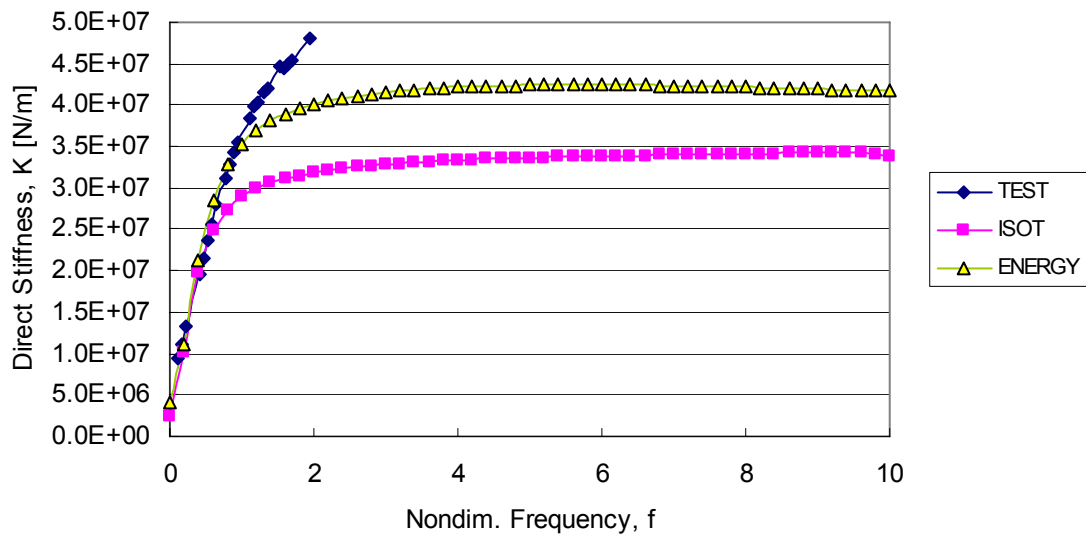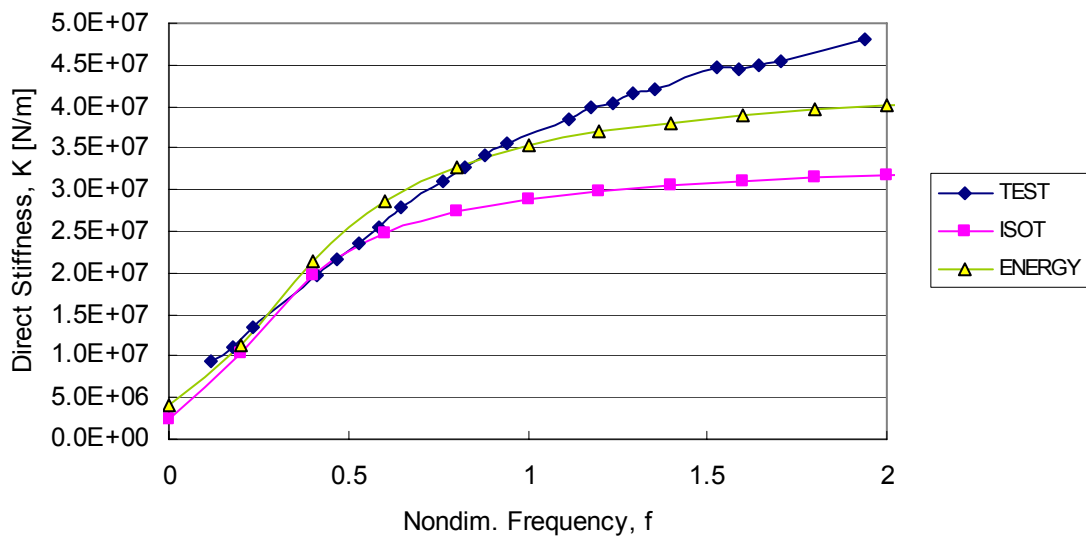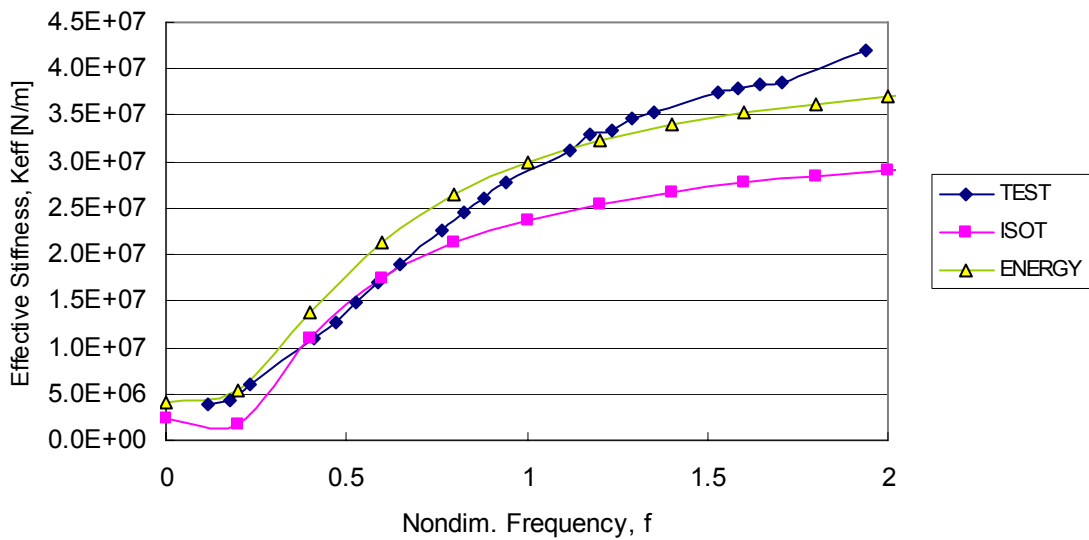**Figure 20 Effective stiffness $K_{eff}(f)$ vs. non-dimensional frequency f for hole-pattern seal (detail)**
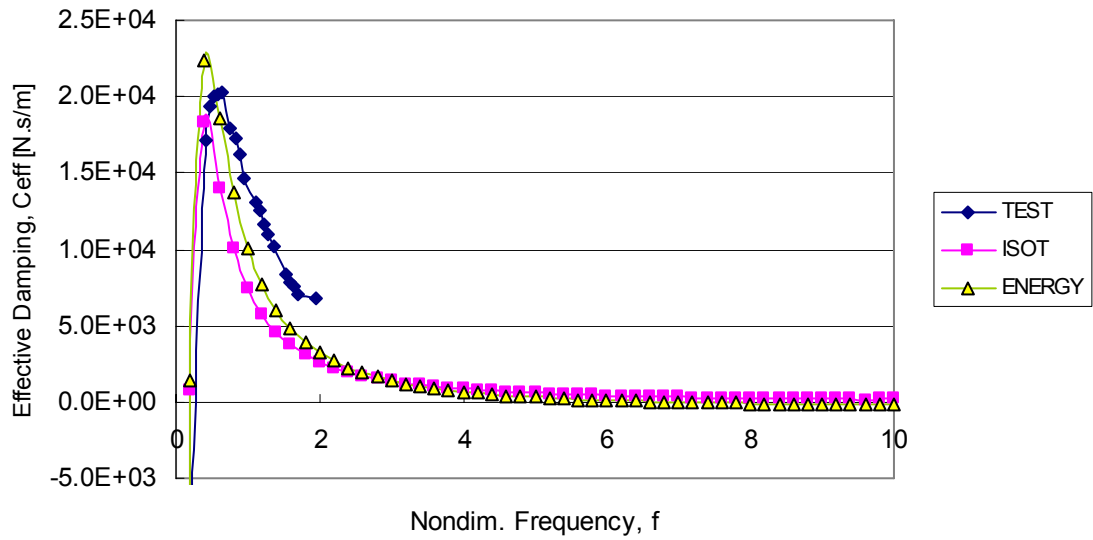
Figure 21 Effective damping $C_{eff}(f)$ vs. non-dimensional frequency f for hole-pattern seal
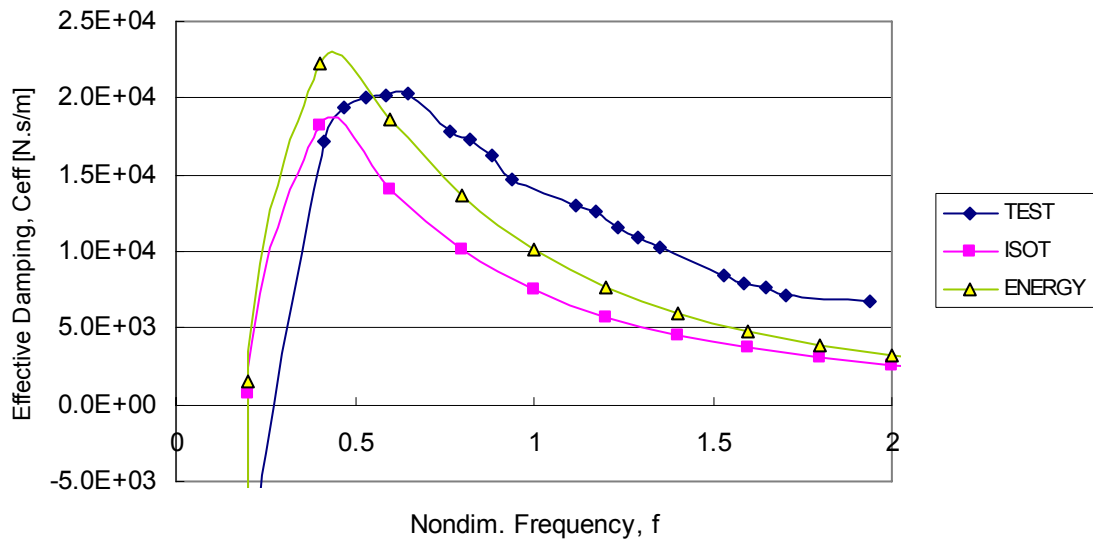
Figure 22 Effective damping $C_{eff}(f)$ vs. non-dimensional frequency f for hole-pattern seal (detail)

5. EFFECT OF REAL GAS PROPERTIES

In this section, example predictions are compared for a methane gas compressor seal with real gas model, 'REAL' and ideal gas model, 'IDEAL'. Here, both models include the energy equation, but 'REAL' uses real gas properties from NIST SUPERTRAPP, while 'IDEAL' gets gas properties from the ideal gas equation of state. 'IDEAL' model is the exact same model as 'ENERGY' in the previous section but named differently for clarity. In Figure 23 through Figure 28, and Figure 29 through Figure 34, comparisons are done with two different ΔP's of 150 bars and 100 bars. The running condition and geometry for this application is:

- P_R = 250 bars
- P_S = 100 bars (Through-flow or series application),
      150 bars (Back-to-back application)
- T_R = 400K
- ω = 10,000 rpm
- D = 250 mm
- L = 150 mm
- C_r = 0.3 mm
- H_d = 2 mm
- γ_c= 0.684
- μ = 2.0E-5 Pa sec
- *Preswirl ratio* = 0
- *Molecular weight* = 16.043
- γ = 1.299
- m_s = -0.1101
- n_s = 0.0785
- m_r = -0.217
- n_r = 0.0586.

Through-flow or series application (P_S = 100 bars, ΔP = 150 bars)
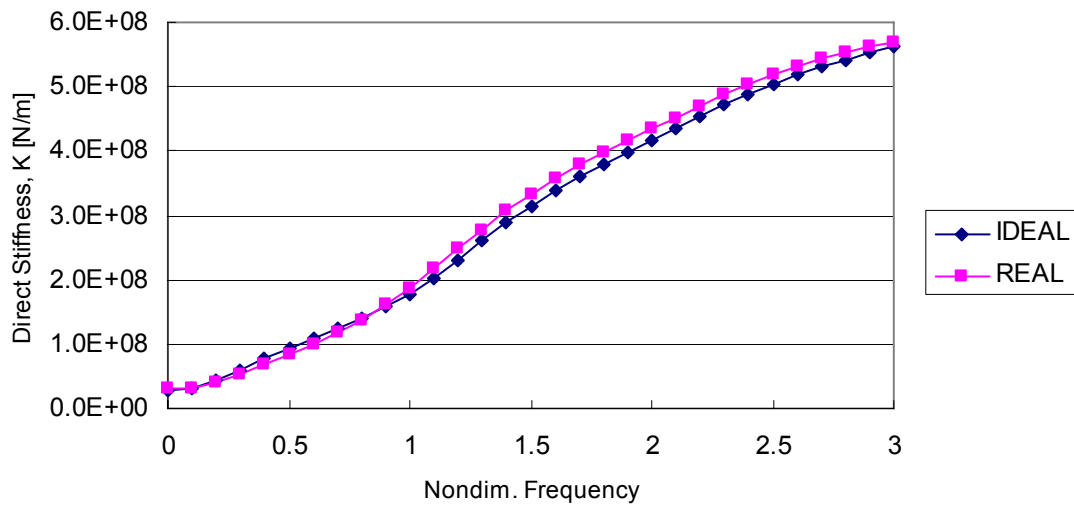
Figure 23 Direct stiffness *K(f)* vs. non-dimensional frequency *f* for through flow application
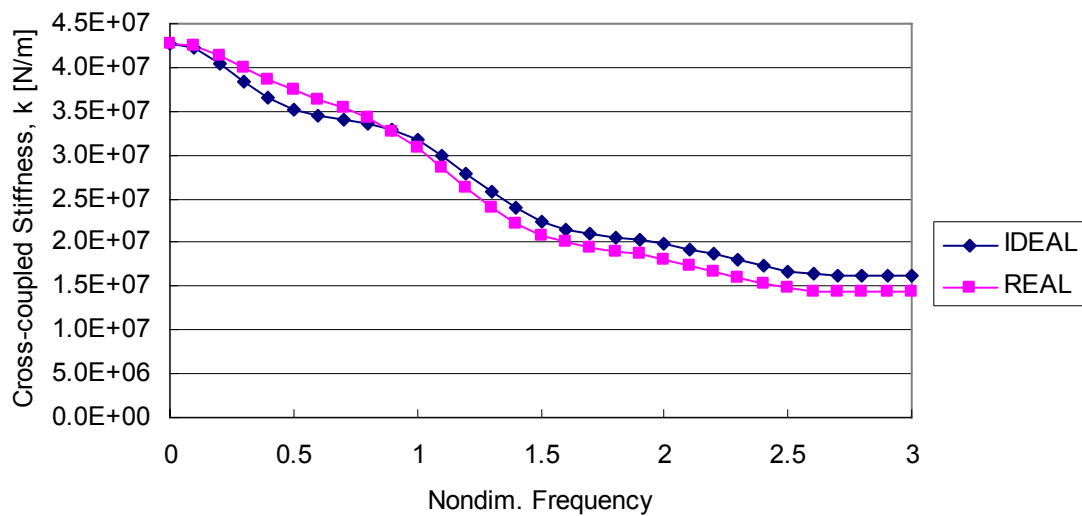
Figure 24 Cross-coupled stiffness *k(f)* vs. non-dimensional frequency *f* for through flow application
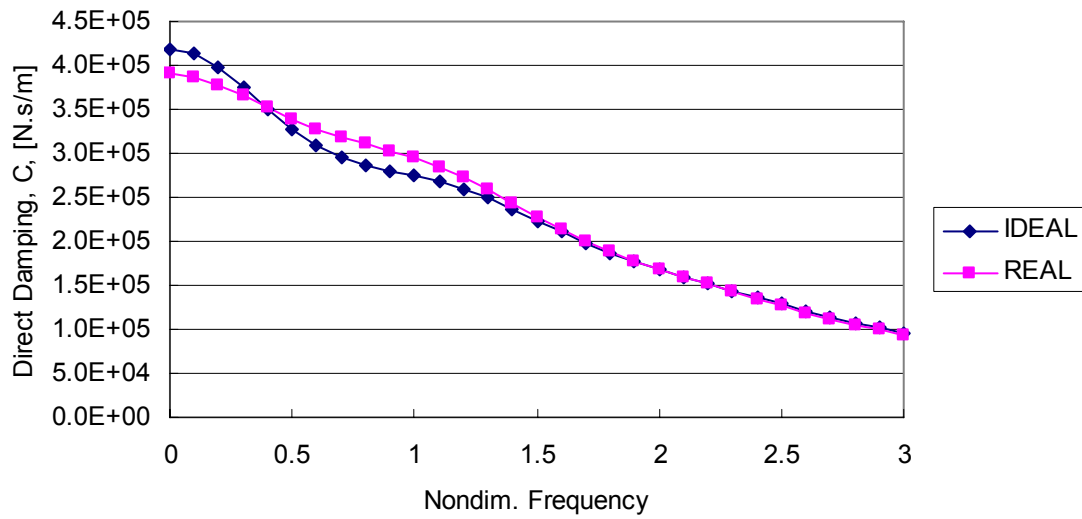
Figure 25 Direct damping *C*(*f*) vs. non-dimensional frequency *f* for through flow application
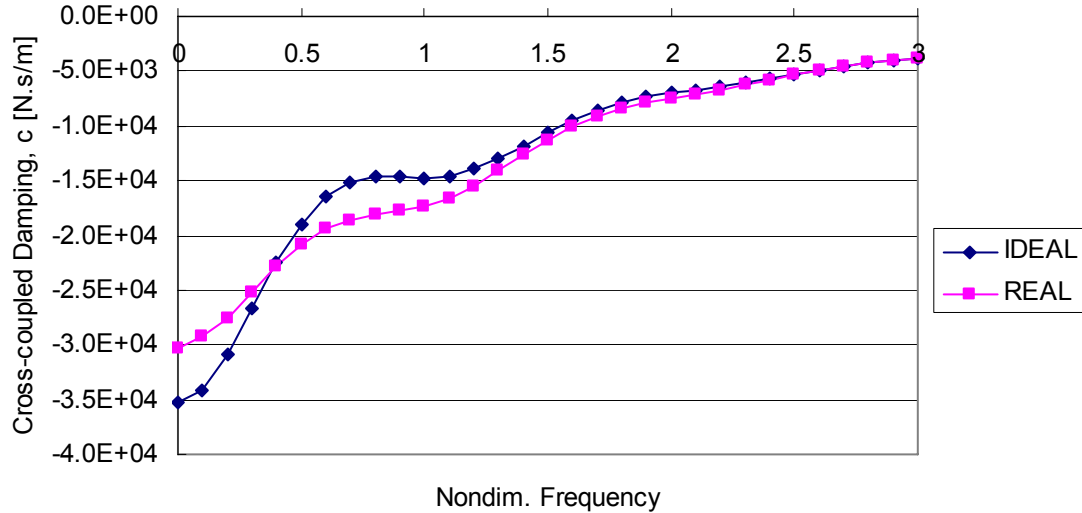
Figure 26 Cross-coupled damping *c*(*f*) vs. non-dimensional frequency *f* for through flow application
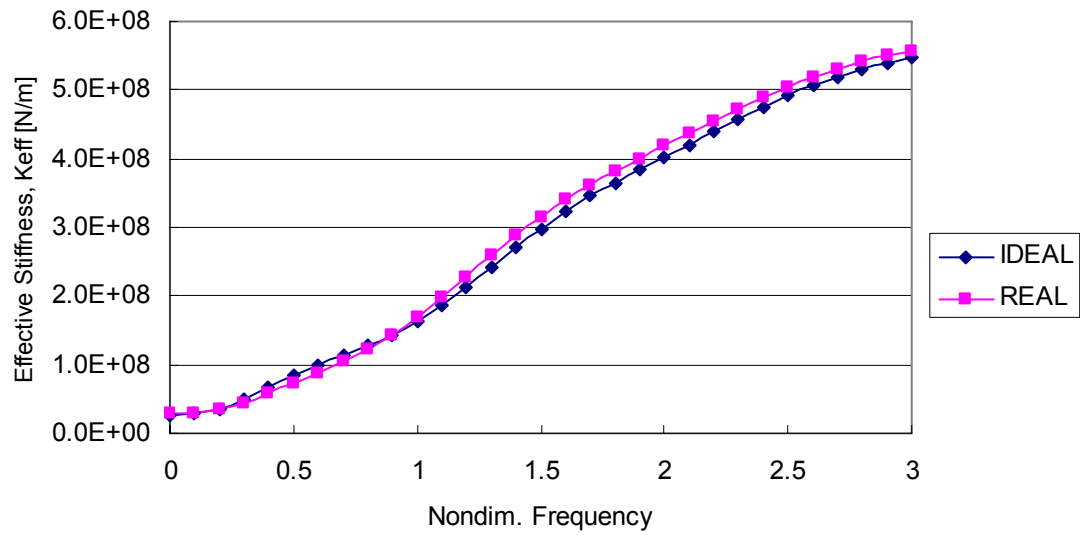
Figure 27 Effective stiffness $K_{eff}(f)$ vs. non-dimensional frequency f for through flow application
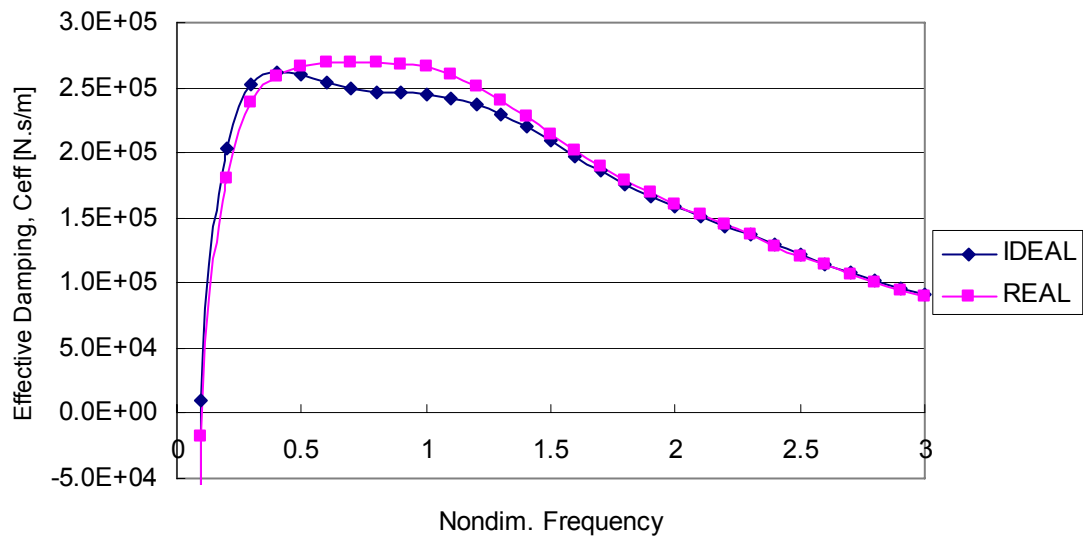
Figure 28 Effective damping $C_{eff}(f)$ vs. non-dimensional frequency f for through flow application

Back-to-back application ($P_S = 150$ bars, $\Delta P = 100$ bars)
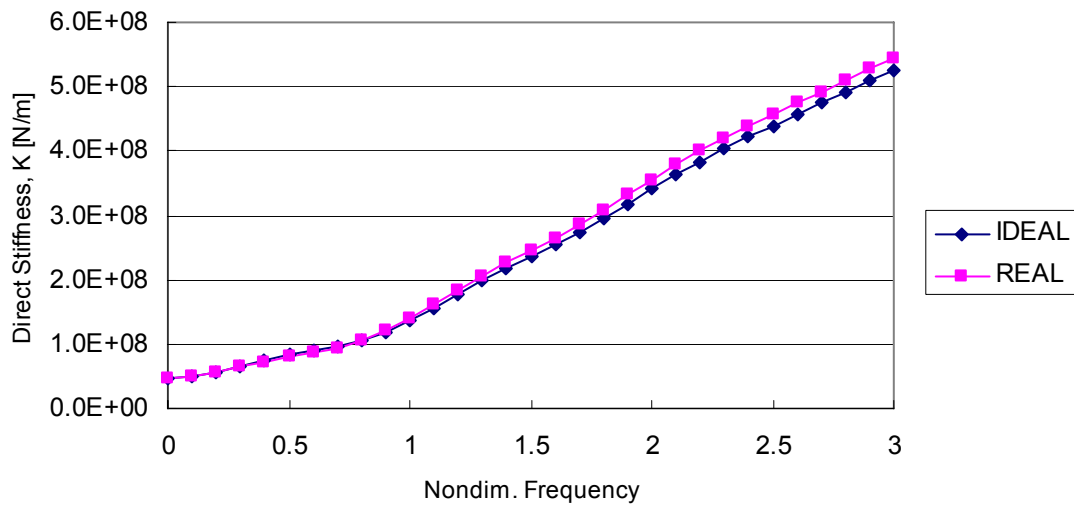
Figure 29 Direct stiffness $K(f)$ vs. non-dimensional frequency f for back-to-back application
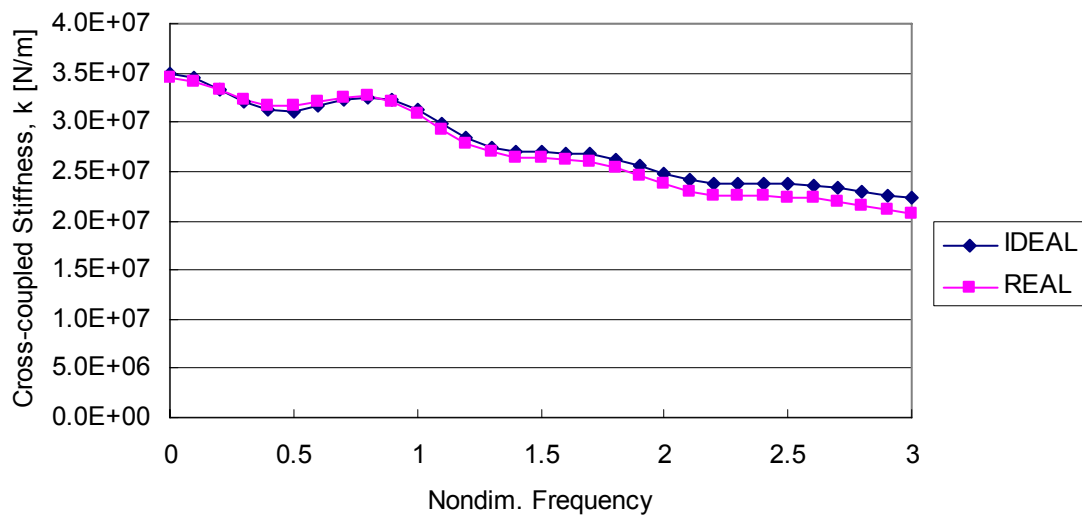
Figure 30 Cross-coupled stiffness $k(f)$ vs. non-dimensional frequency f for back-to-back application
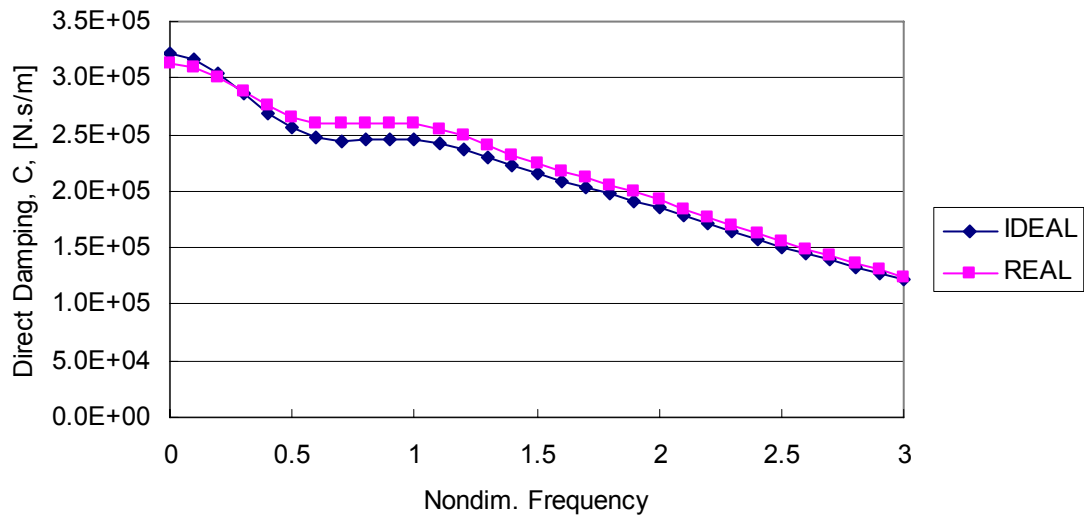
Figure 31 Direct damping *C*(*f*) vs. non-dimensional frequency *f* for back-to-back application
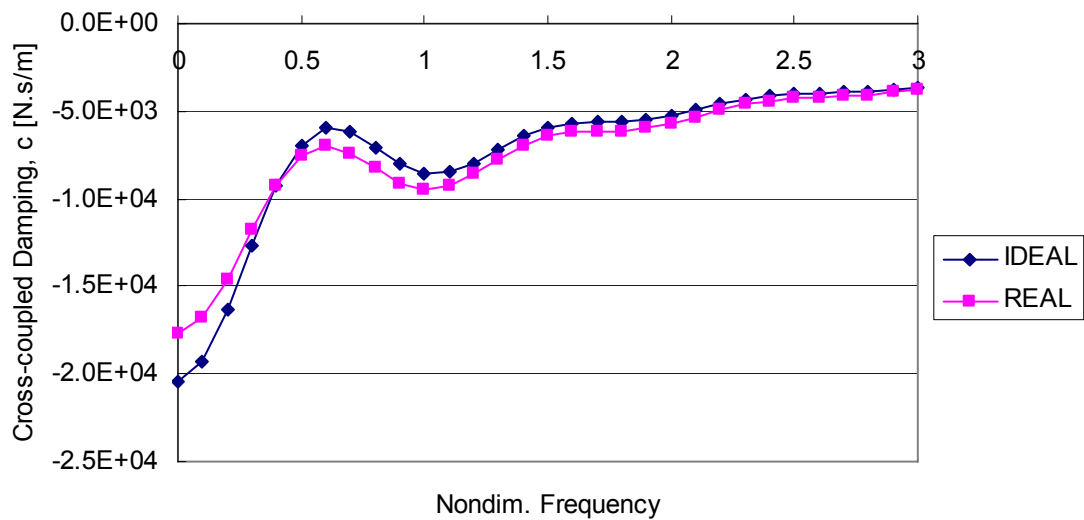
Figure 32 Cross-coupled damping *c*(*f*) vs. non-dimensional frequency *f* for back-to-back application
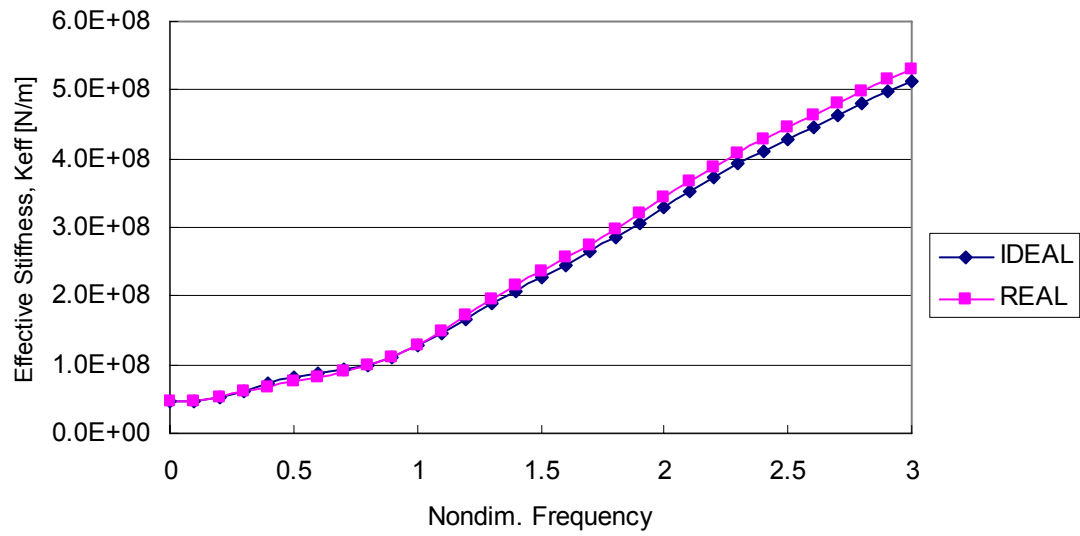
Figure 33 Effective stiffness $K_{eff}(f)$ vs. non-dimensional frequency f for back-to-back application
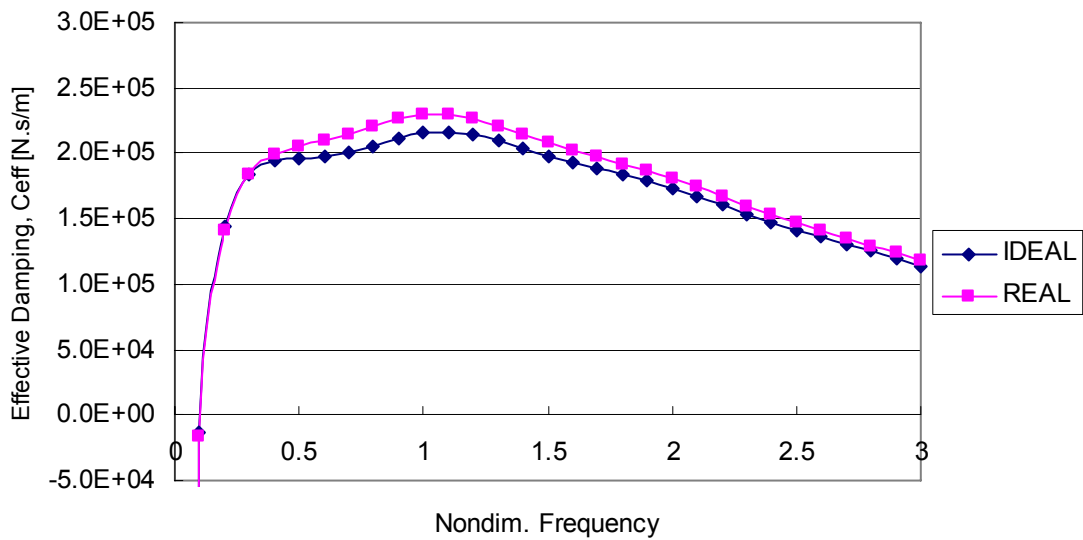
Figure 34 Effective damping $C_{eff}(f)$ vs. non-dimensional frequency f for back-to-back application

The plots show that predictions for 'IDEAL' and 'REAL' differ slightly. IDEAL tends to predict less direct stiffness at running speed and higher frequencies, and predict less effective damping at the non-dimensional frequency ranges of $0.5 < f < 1.5$ (through-flow) and $0.5 < f < 2$ (back-to-back). The difference of direct damping at zero frequency is 2-5%. The crossover frequency, which is the frequency that effective damping turns from negative to positive, does not change much between two models.

6. EFFECT OF STATOR-HOLE-DEPTH VARIATION

In this section, the effect of varying hole-depth of seal is examined. The purpose of this study is finding the most helpful configuration of hole-depth variation. For trial configurations of $H_d(z)$, five simple functions are presented for linear, convex, concave, convex-and-concave, and concave-and-convex curves. Each function will form two curves in each case of $H_{d,in} < H_{d,ex}$ and $H_{d,in} > H_{d,ex}$. The hole-depth equations and schematics are provided in Table 4. A unique name is assigned to each function, which appears in the first column of Table 4. The configuration will be named with combinations of function name and 'IN' for increasing or 'DE' for decreasing.

Rotordynamic coefficients are predicted with 'ISOT' model of section 4, because 'ISOT' gives the nicest curves for frequency dependent rotordynamic coefficients, and as shown in section 4, hole-pattern seals at frequency of running speed and below are fairly close to 'ENERGY' model. The prediction is performed in the same condition of section 4 except H_d and Running Speed.

- *Running Speed* = 15,200 rpm
- 'ISOT' H_d = 3.3 mm
- 'IN' $H_{d,in}$ = 1.65 mm, $H_{d,ex}$ = 4.95 mm
- 'DE' $H_{d,in}$ = 4.95 mm, $H_{d,ex}$ = 1.65 mm

This arrangement for $H_{d,in}$ and $H_{d,ex}$ causes the seals to have approximately the same average hole depth. Predictions of effective damping and direct stiffness coefficients with eleven configurations of $H_d(z)$ are plotted in Figure 35 and Figure 36 respectively.

Table 4 Trial configurations of H_d variation

	'IN' $\quad H_{d,in} < H_{d,ex}$	'DE' $\quad H_{d,in} > H_{d,ex}$
'LINEAR' $$H_d = H_{d,in} + \frac{H_{d,ex} - H_{d,in}}{L} Z$$		
'SQUARE' $$H_d = H_{d,in} + \frac{H_{d,ex} - H_{d,in}}{L^2} Z^2$$		
'SQRT' $$H_d = H_{d,in} + \frac{H_{d,ex} - H_{d,in}}{\sqrt{L}} \sqrt{Z}$$		
'COS' $$H_d = \frac{H_{d,in} - H_{d,ex}}{2} \cos \frac{\pi Z}{L}$$ $$+ \frac{H_{d,in} + H_{d,ex}}{2}$$		
'ARCCOS' $$H_d = \frac{H_{d,ex} - H_{d,in}}{\pi} \cos^{-1}\left(1 - \frac{2Z}{L}\right)$$ $$+ H_{d,in}$$ $$\left(0 \le \cos^{-1}\left(1 - \frac{2Z}{L}\right) \le \pi\right)$$		
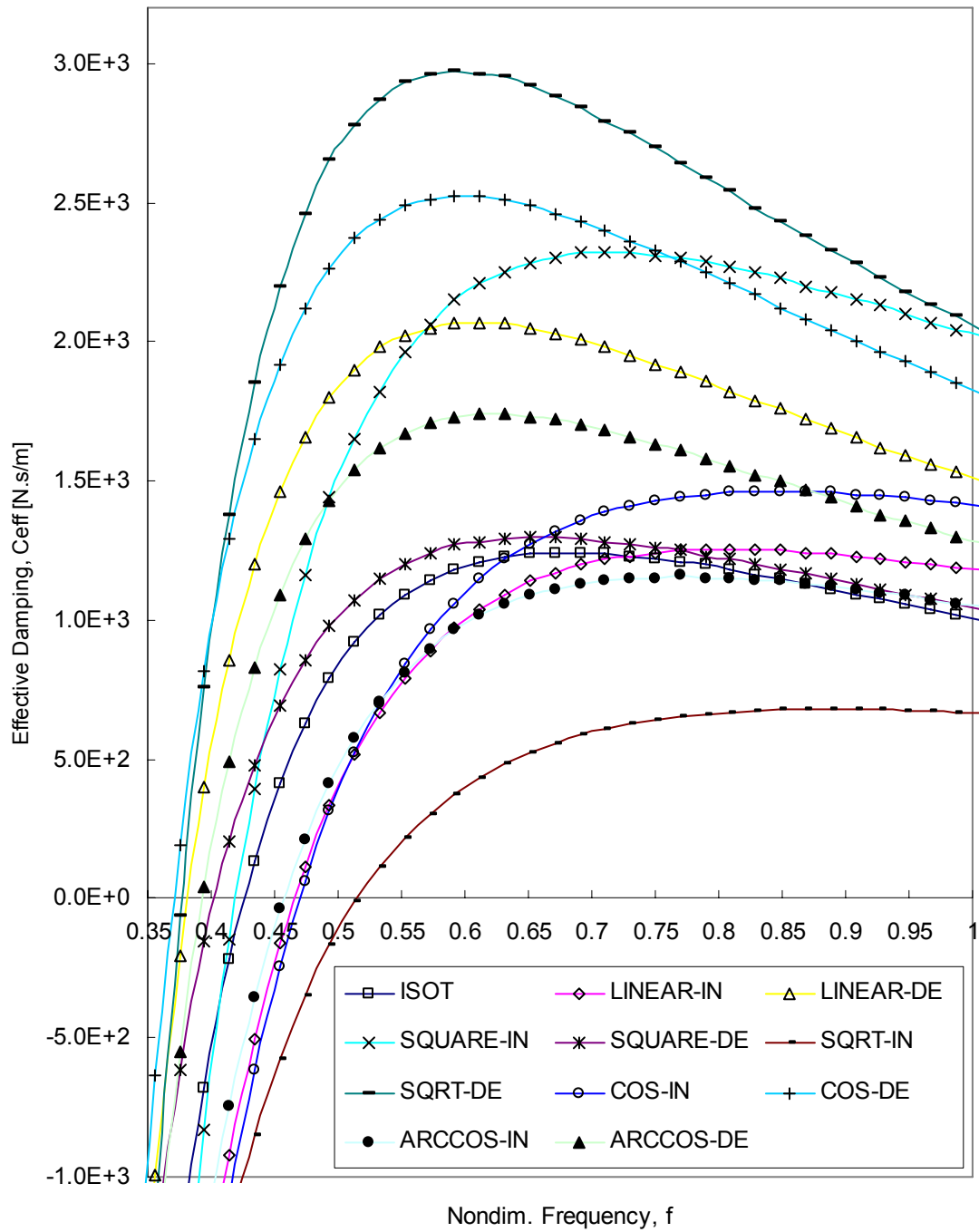
Figure 35 Effective damping $C_{eff}(f)$ vs. non-dimensional frequency f for various hole-depth variations
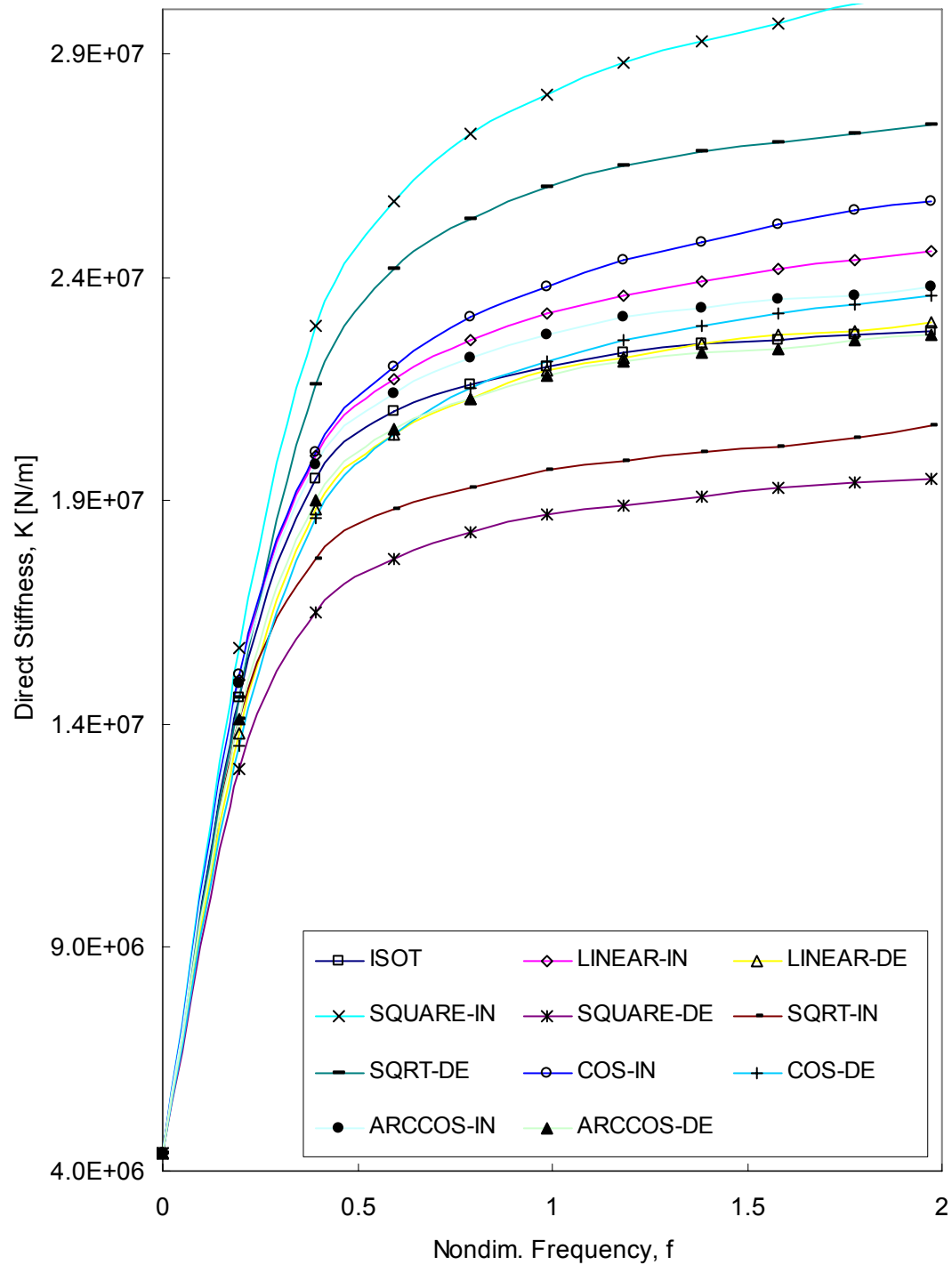
Figure 36 Direct stiffness $K(f)$ vs. non-dimensional frequency f for various hole-depth variations

Figure 35 and Figure 36 show that varying the hole-depth axially has a dramatic impact on the frequency dependent rotordynamic coefficients. The crossover frequency for the best variable-depth seal drops to 0.37 from 0.42 for the constant hole-depth case. The peak damping increases from 1,200 Ns/m to 3,000 Ns/m, an increase of 125%. The 'SQRT-DE' configuration has highest effective damping at wide range of frequency, and its crossover frequency is one of the lowest. The 'COS-DE' configuration has high effective damping, but direct stiffness is a bit lower than average. The best choice among given configuration is 'SQRT-DE'.

7. EFFECT OF DEEP ANNULAR GROOVE

According to Childs [12], as a liquid seal gets longer, its direct stiffness tends to decrease, and become negative. To resolve this problem, some pump company put a deep annular groove in the seal to break a long seal into shorter seals.

A deep annular groove makes the pressure not perturbed at the groove; therefore, a grooved seal can be regarded as two consecutive seals with the same leakage. Figure 37 shows a grooved hole-pattern seal. The grooved-seal analysis is nothing but successive solutions of two seals, sharing pressure, temperature and circumferential velocity at the groove, namely, at the exit of seal #1 and the inlet of seal #2. To find mass flow rate, pressure at the groove is used for comparison. The algorithm for grooved-seal is as following. Firstly, the zeroth order equation of seal #1 is solved with ΔP_{temp} which is an half of given ΔP, and the mass flow rate is stored. Now the discharge pressure, exit temperature and exit circumferential velocity of the seal #1 substitute the reservoir pressure, inlet temperature and preswirl of seal #2 respectively, and the zeroth order solution of seal #2 is computed. The mass flow rates of seal #1 and seal #2 are compared to be equal, and this block of calculation is repeated with different ΔP_{temp}'s until the difference of mass flow rates are within the given tolerance. Finally, both seals are calculated with the found pressure at the groove, and the rotordynamic coefficients are summed up for entire grooved seal solution.

In this section, the running condition and seal geometry for tests and predictions are the same as Section 4 except for following data:

- $P_R = 70$ bar
- $P_S = 18.9$ bar
- $\omega = 10,200$ rpm
- $C_r = 0.1$ mm
- *Preswirl* = 0
- *Groove width* = 5.5 mm
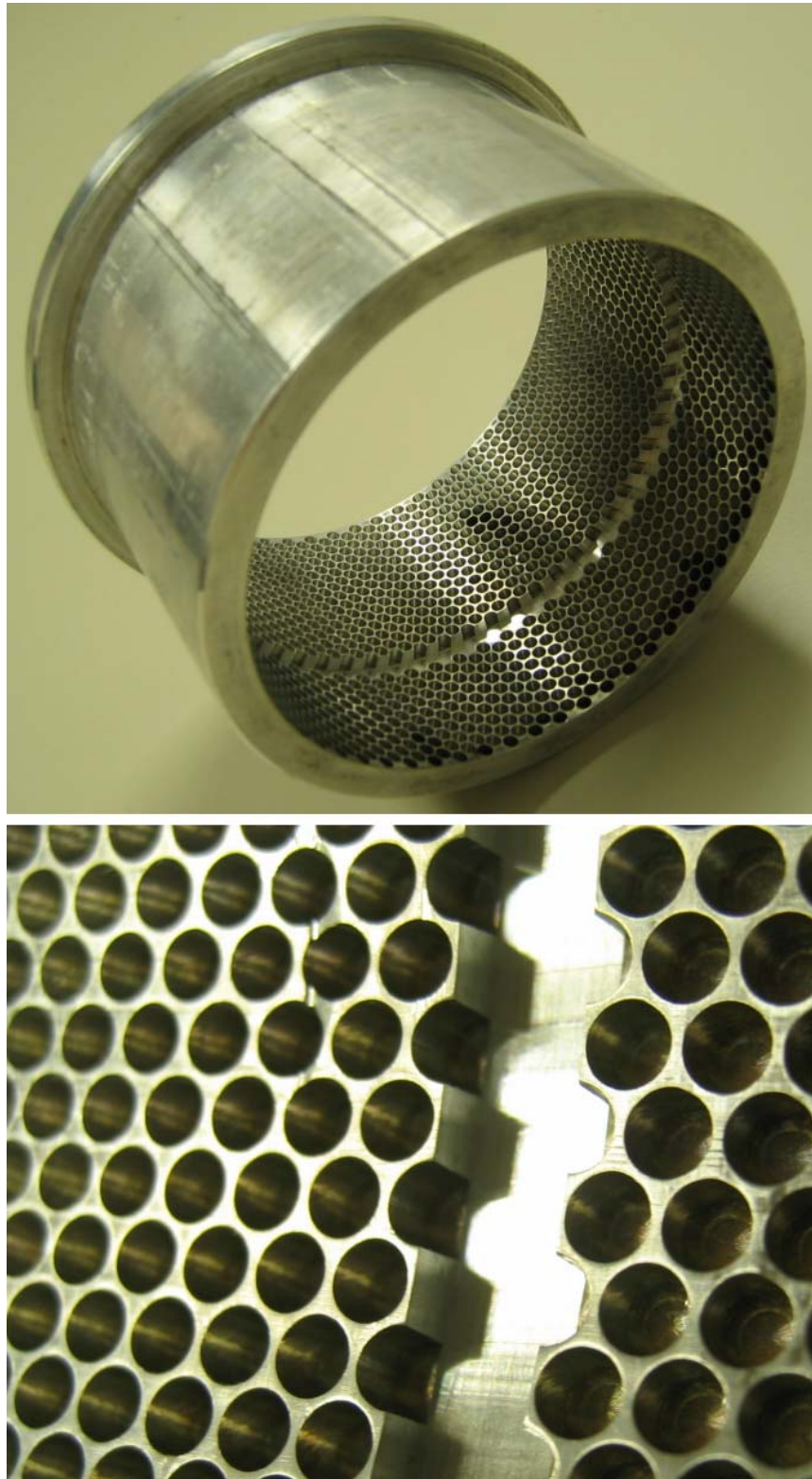
Figure 37 Grooved hole-pattern seal

7.1 Optimal Groove Position

The first issue for this study is the optimal groove position. The primary purpose of putting a groove in an annular seal is elevating stiffness at zero frequency. To determine the optimal position, the code is run for 10 groove positions that are equally distributed through seal, then effective stiffness is plotted to determine the optimal position of groove. Frequency dependent rotordynamic coefficients for grooved seal are computed and compared with test data. The position of a groove is defined as,

$$(groove\ position) = \frac{(length\ of\ seal\,\#1)}{(length\ of\ seal\#1) + (length\ of\ seal\#2)} = \frac{(length\ of\ seal\,\#1)}{L - (groove\ width)}. \quad (32)$$
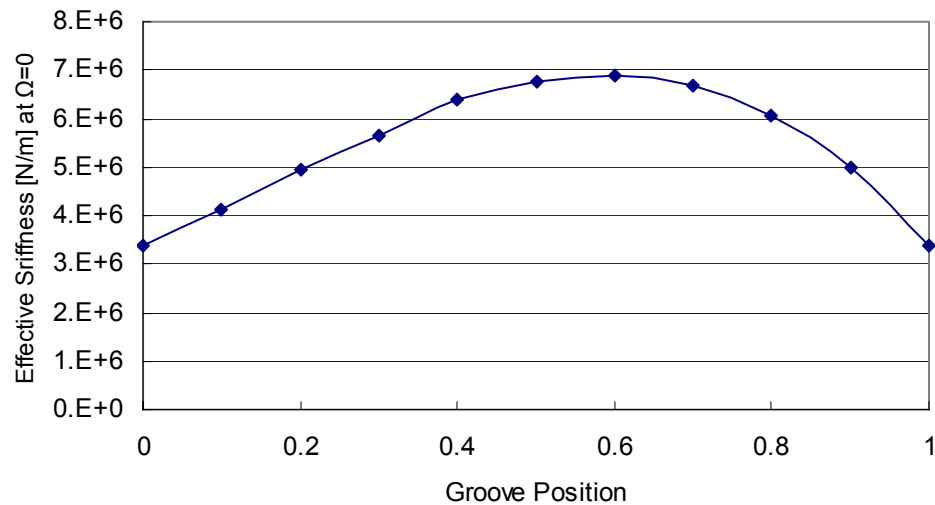
Figure 38 Effective stiffness at zero precessional frequency vs. non-dimensional groove position

Figure 38 shows that putting a groove at 60% from the inlet of a seal is most helpful. The comparison between prediction and experiment is done with two seals grooved at 60%.

7.2 Grooved Seal Analysis

For each case of un-grooved and grooved, frequency-dependent direct stiffness $K(f)$, effective stiffness $K_{eff}(f)$, direct damping $C(f)$ and effective damping $C_{eff}(f)$ are measured, and predicted with 'ENERGY' model of section 4. The plots in Figure 39 through Figure 42 are named as,

- 'TEST': test result for normal hole-pattern seal,
- 'TEST-G': test result for grooved-seal,
- 'ENERGY': predicted data for normal hole-pattern seal with 'ENERGY',
- 'ENERGY-G': predicted data for grooved-seal with 'ENERGY'.

As expected, at zero frequency, direct stiffness of grooved-seal is higher than that of un-grooved seal, and they cross as increasing frequency. Even though test results do not show stiffness at zero frequency, they are about to cross each other. Once a seal is grooved, the seal loses large amount of damping below running speed. 'ENERGY' is predicting crossover frequency 40% (un-grooved) and 50% (grooved) lower.

Leakage predictions for un-grooved and grooved seals are compared with test results in Figure 43. Leakage is normalized to flow coefficient. The flow coefficient is defined as,

$$\Phi = \frac{\dot{m}\sqrt{RT}}{\pi D C_r \Delta P} \tag{33}$$

Leakage is well predicted with the 'ENERGY' code. Both of 'TEST' and 'ENERGY' show that grooved-seal has a bit higher leakage, but the leakage increase due to a groove is not significant.
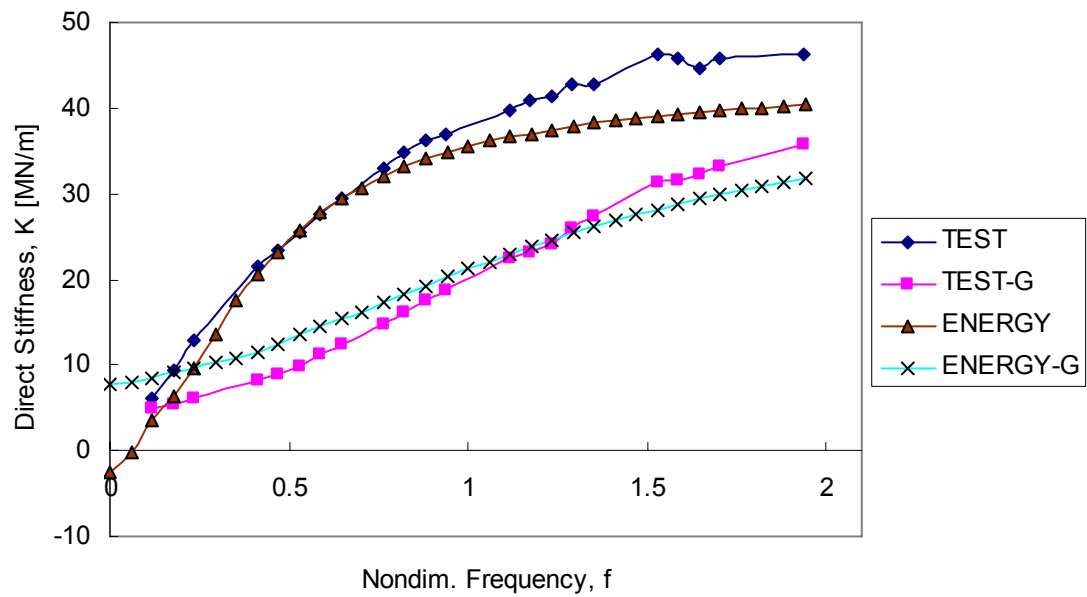
Figure 39 Direct stiffness *K*(*f*) vs. non-dimensional frequency *f* for un-grooved and grooved seals (*ω* = 336.67 Hz)
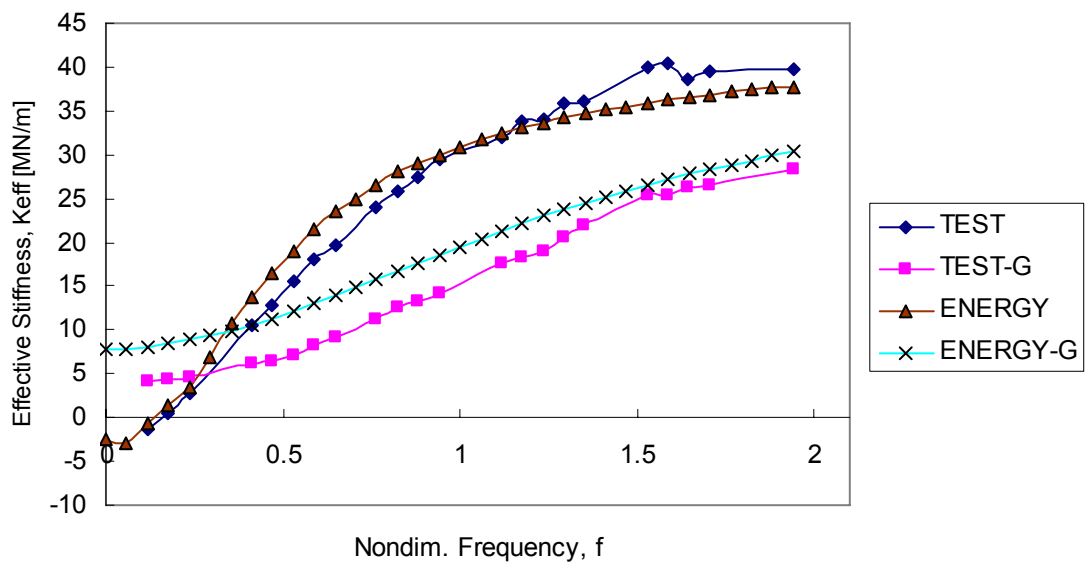
Figure 40 Effective stiffness *K*_{*eff*}(*f*) vs. non-dimensional frequency *f* for un-grooved and grooved seals (*ω* = 336.67 Hz)
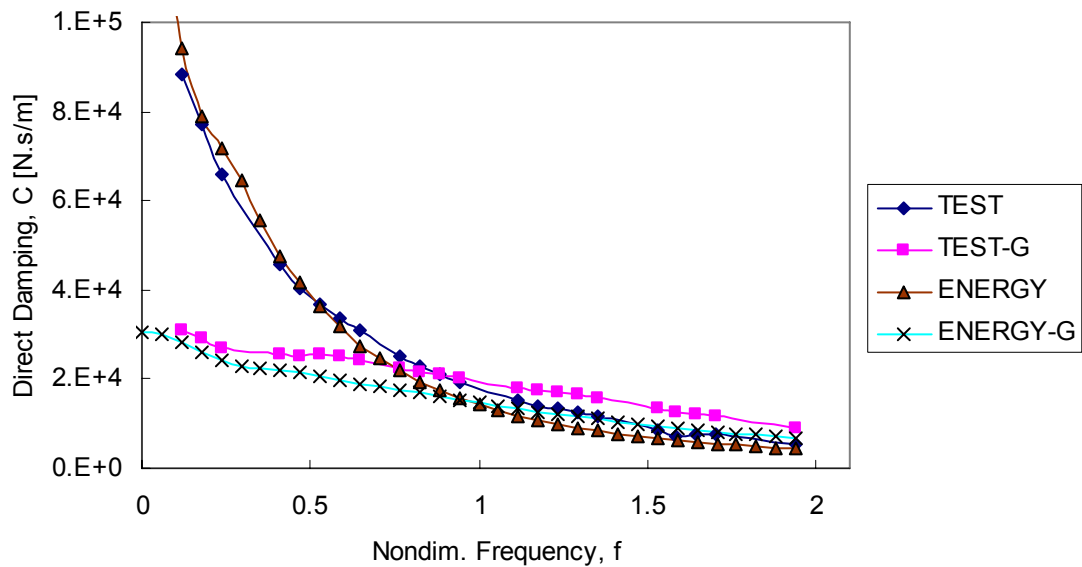
Figure 41 Direct damping $C(f)$ vs. non-dimensional frequency f for un-grooved and grooved seals ($\omega = 336.67$ Hz)
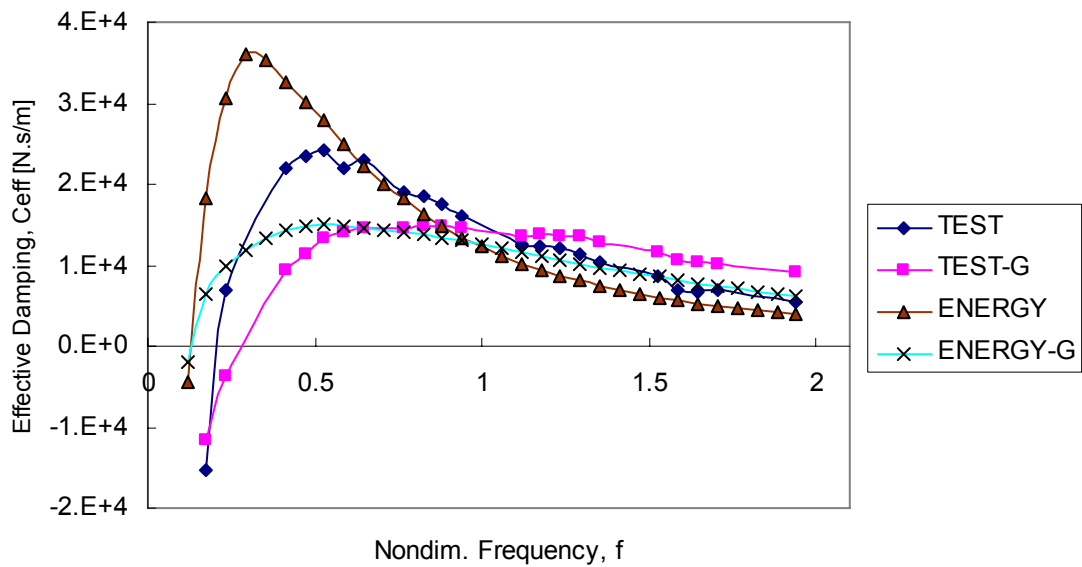
Figure 42 Effective damping $C_{eff}(f)$ vs. non-dimensional frequency f for un-grooved and grooved seals ($\omega = 336.67$ Hz)
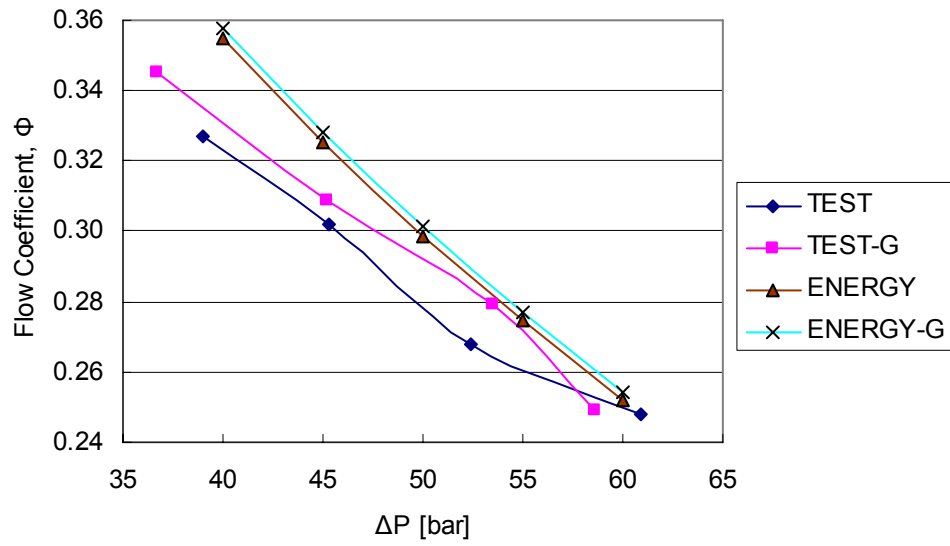
Figure 43 Flow coefficient Φ vs. Δ*P* for un-grooved and grooved seals

9. SUMMARY

Modifications to gas seal analysis of Kleynhans and Childs [6] are presented in this thesis. This study showed that considering temperature change of seal flow is important. Static solution and dynamic coefficients are moderately affected by temperature change. Including real gas properties is also important especially for high pressure gas application.

The hole-pattern depth variation turned out to be also an influencing parameter of seal prediction. Effective damping and direct stiffness coefficients are dramatically changed with different configuration of hole-depth variation, which can cause significant change of seal performance. There is no explicit relationship found between change of rotordynamic coefficients and hole-depth variation geometry.

Grooved seal is well predicted with given model through zero to running speed frequency range. Low stiffness problem can be resolved at low frequency range, but the seal loses direct stiffness and slightly gains leakage rate.

REFERENCES

[1] Childs, D., and Moyer, D., 1985, "Vibration Characteristics of the HPOTP (High-Pressure Oxygen Turbopump) of the SSME (Space Shuttle Main Engine)," ASME Journal of Engineering for Gas Turbine and Power, **107**, pp. 152-159.

[2] Yu, Z., and Childs, D., 1998, "A Comparison of Experimental Rotordynamic Coefficients and Leakage Characteristics Between Hole-Pattern Gas Damper Seals and a Honeycomb Seal," ASME Journal of Engineering for Gas Turbine and Power, **120**(4), pp. 778-783.

[3] Nelson, C. C., 1984, "Analysis for Leakage and Rotordynamic Coefficients of Surface-Roughened Tapered Annular Gas Seals," ASME Journal of Engineering for Gas Turbines and Power, **106**, pp. 927-934.

[4] Nelson, C. C., 1985, "Rotordynamic Coefficients for Compressible Flow in Tapered Annular Seals," ASME Journal of Tribology, **107**, pp. 318-325.

[5] Ha, T.-W., and Childs, D., 1994, "Annular Honeycomb-Stator Turbulent Gas Seal Analysis Using a New Friction-Factor Model Based on Flat Plate Tests," ASME Journal of Tribology, **116**, pp. 352-360.

[6] Kleynhans, G., and Childs, D., 1997, "The Acoustic Influence of Cell Depth on the Rotordynamic Characteristics of Smooth-Rotor/Honeycomb-Stator Annular Gas Seals," ASME Journal of Engineering for Gas Turbines and Power, **119**, pp. 949-957.

[7] Childs, D., and Wade, J., 2004, "Rotordynamic-Coefficient and Leakage Characteristics for Hole-Pattern-Stator Annular Gas Seals−Measurements Versus Predictions," ASME Journal of Tribology, **126**, pp. 326-333.

[8] Huber, M. L., 2003, NIST Thermophysical Properties of Hydrocarbon Mixtures Database (SUPERTRAPP), Version 3.1, U. S. Department of Commerce, National Institute of Standards and Technology, Standard Reference Data Program, Gaithersburg, MD.

[9] D'Souza, R., and Childs, D., 2002, "A Comparison of Rotordynamic-Coefficient Predictions of Annular Honeycomb Gas Seals Using Different Friction-Factor Models," ASME Journal of Tribology, **124**, pp. 524-529.

[10] Kerr, B. G., 2004, "Experimental and Theoretical Rotordynamic Coefficients and Leakage of Straight Smooth Annular Gas Seals," M.S. thesis, Department of Mechanical Engineering, Texas A&M University, College Station, TX.

[11] Childs, D., and Fayolle, P., 1999, "Test Results for Liquid 'Damper' Seals Using a Round-Hole Roughness Pattern for the Stators," ASME Journal of Tribology, **121**, pp. 42-49.

[12] Childs, D., 1993, *Turbomachinery Rotordynamics*: *Phenomena, Modeling, & Analysis*, John Wiley & Sons, New York.

APPENDIX A
SOLUTION OF GOVERNING EQUATIONS

A.1. Non-dimensional Governing Equations

Non-dimensionalized parameters are defined as following:

$$w = \frac{W}{R\omega} \tag{A1}$$

$$p = \frac{P}{P_R} \tag{A2}$$

$$u = \frac{U}{R\omega} \tag{A3}$$

$$\tilde{\rho} = \frac{\rho}{\rho_R} \tag{A4}$$

$$h = \frac{H}{C_r} \tag{A5}$$

$$h_d = \frac{H_d}{C_r} \tag{A6}$$

$$c_r = \frac{C_r}{R} \tag{A7}$$

$$l = \frac{L}{R} \tag{A8}$$

$$z = \frac{Z}{L} \tag{A9}$$

$$\tau = t\omega \tag{A10}$$

$$p_S = \frac{P_S}{P_R} \tag{A11}$$

$$\tilde{\hat{u}} = \frac{\hat{u}}{\hat{u}_R}. \tag{A12}$$

Non-dimensionalized governing equations for the combined control volume is expressed
for

Continuity:

$$\frac{\partial}{\partial \tau}\left[\tilde{\rho}(h+\gamma_c h_d)\right] + \frac{\partial}{\partial \theta}\left(\tilde{\rho}uh\right) + \frac{1}{l}\frac{\partial}{\partial z}\left(\tilde{\rho}wh\right) = 0 \tag{A13}$$

Axial Momentum:

$$-\frac{P_c}{l\tilde{\rho}}\frac{\partial p}{\partial z} = \frac{w}{2c_r h}\left(\sqrt{u^2+w^2}f_s + \sqrt{(u-1)^2+w^2}f_r\right) + \frac{Dw}{D\tau} \tag{A14}$$

Circumferential Momentum:

$$-\frac{P_c}{\tilde{\rho}}\frac{\partial p}{\partial \theta} = \frac{1}{2c_r h}\left(u\sqrt{u^2+w^2}f_s + (u-1)\sqrt{(u-1)^2+w^2}f_r\right) + \frac{Du}{D\tau} \tag{A15}$$

Energy - Real Gas:

$$\begin{aligned}
\frac{p}{h}\frac{\partial h}{\partial \tau} = {}& \hat{u}_c\tilde{\rho}\frac{D\tilde{\tilde{u}}}{D\tau} - \frac{p}{\tilde{\rho}}\frac{D\tilde{\rho}}{D\tau} \\
& + \frac{\gamma_c h_d}{h}\left[\hat{u}_c\tilde{\rho}\frac{\partial \tilde{\tilde{u}}}{\partial \tau} - \frac{p}{\tilde{\rho}}\frac{\partial \tilde{\rho}}{\partial \tau} + \frac{\tilde{\rho}}{P_c}\left(u\frac{\partial u}{\partial \tau} + w\frac{\partial w}{\partial \tau}\right)\right] \\
& - \frac{\tilde{\rho}}{2P_c c_r h}\left[\left(\sqrt{u^2+w^2}\right)^3 f_s + \left(\sqrt{(u-1)^2+w^2}\right)^3 f_r\right]
\end{aligned} \tag{A16}$$

Energy - Ideal Gas:

$$\begin{aligned}
\frac{p}{h}\frac{\partial h}{\partial \tau} = {}& \frac{1}{Z_c(\gamma-1)}\frac{Dp}{D\tau} - \left(\frac{1}{Z_c(\gamma-1)}+1\right)\frac{p}{\tilde{\rho}}\frac{D\tilde{\rho}}{D\tau} \\
& + \frac{\gamma_c h_d}{h}\left[\frac{1}{Z_c(\gamma-1)}\frac{\partial p}{\partial \tau} - \left(\frac{1}{Z_c(\gamma-1)}+1\right)\frac{p}{\tilde{\rho}}\frac{\partial \tilde{\rho}}{\partial \tau} + \frac{\tilde{\rho}}{P_c}\left(u\frac{\partial u}{\partial \tau} + w\frac{\partial w}{\partial \tau}\right)\right] \\
& - \frac{\tilde{\rho}}{2P_c c_r h}\left[\left(\sqrt{u^2+w^2}\right)^3 f_s + \left(\sqrt{(u-1)^2+w^2}\right)^3 f_r\right]
\end{aligned} \tag{A17}$$

where,

$$\frac{D}{D\tau} = \frac{\partial}{\partial \tau} + u\frac{\partial}{\partial \theta} + \frac{w}{l}\frac{\partial}{\partial z} \tag{A18}$$

$$P_c = \frac{P_R}{\rho_R(R\omega)^2} \tag{A19}$$

$$\hat{u}_c = \frac{\hat{u}_R \rho_R}{p_R}. \tag{A20}$$

Non-dimensionalized hole-pattern depth variations are expressed for,

a. linear:
$$h_d = h_{d,in} + \left(h_{d,ex} - h_{d,in} \right) z \qquad (A21)$$

b. square:
$$h_d = h_{d,in} + \left(h_{d,ex} - h_{d,in} \right) z^2 \qquad (A22)$$

c. sqrt:
$$h_d = h_{d,in} + \left(h_{d,ex} - h_{d,in} \right) \sqrt{z} \qquad (A23)$$

d. cos:
$$h_d = \frac{h_{d,in} - h_{d,ex}}{2} \cos\left(\pi z \right) + \frac{h_{d,in} + h_{d,ex}}{2} \qquad (A24)$$

e. arccos:
$$h_d = \frac{h_{d,ex} - h_{d,in}}{\pi} \cos^{-1}\left(1 - 2z \right) + h_{d,in}. \qquad (A25)$$

Non-dimensional entrance loss and exit recovery equations are:

$$1 - p(0) = \frac{1+\xi}{2P_c} \tilde{\rho}(0) w^2(0) \qquad (A26)$$

$$p(0) = \tilde{\rho}^{\gamma}(0) \qquad (A27)$$

$$p(1) - p_S = -\frac{1-\xi_e}{2P_c} \tilde{\rho}(1) w^2(1) \qquad (A28)$$

A.2. Perturbation Analysis

Perturbation variables are introduced here,

$$h = h_0 + \varepsilon h_1 \qquad (A29)$$

$$w = w_0 + \varepsilon w_1 \qquad (A30)$$

$$p = p_0 + \varepsilon p_1 \qquad (A31)$$

$$u = u_0 + \varepsilon u_1 \qquad (A32)$$

$$\tilde{\rho} = \tilde{\rho}_0 + \varepsilon \tilde{\rho}_1 \qquad (A33)$$

$$\tilde{u} = \tilde{u}_0 + \varepsilon \tilde{u}_1 \qquad (A34)$$

where, ε is the perturbed eccentricity ratio, which is very small number. With the variables (A29)-(A34), the governing equations are separated into zeroth and first order perturbation equations.

A.2.1 Zeroth Order Equations

Zeroth order perturbation equations are given here,

Continuity:

$$0 = \tilde{\rho}_0 w_0 \frac{\partial h_0}{\partial z} + w_0 h_0 \frac{\partial \tilde{\rho}_0}{\partial z} + \tilde{\rho}_0 h_0 \frac{\partial w_0}{\partial z} \tag{A35}$$

Axial momentum:

$$-\frac{P_c}{l\tilde{\rho}_0} \frac{\partial p_0}{\partial z} = \frac{w_0}{2c_r h_0}\left(u_{s0} f_{s0} + u_{r0} f_{r0}\right) + \frac{w_0}{l} \frac{\partial w_0}{\partial z} \tag{A36}$$

Circumferential momentum:

$$0 = \frac{1}{2c_r h_0}\left(u_0 u_{s0} f_{s0} + (u_0 - 1)u_{r0} f_{r0}\right) + \frac{w_0}{l} \frac{\partial u_0}{\partial z} \tag{A37}$$

Energy - Real Gas:

$$0 = \frac{\hat{u}_c \tilde{\rho}_0 w_0}{l} \frac{\partial \tilde{u}_0}{\partial p_0} \frac{\partial p_0}{\partial z} + \left(\hat{u}_c \tilde{\rho}_0 \frac{\partial \tilde{u}_0}{\partial \tilde{\rho}_0} - \frac{p_0}{\tilde{\rho}_0}\right) \frac{w_0}{l} \frac{\partial \tilde{\rho}_0}{\partial z} - \frac{\tilde{\rho}_0}{2P_c c_r h_0}\left(u_{s0}{}^3 f_{s0} + u_{r0}{}^3 f_{r0}\right) \tag{A38}$$

Energy - Ideal Gas:

$$0 = \frac{w_0}{lZ_c(\gamma - 1)} \frac{\partial p_0}{\partial z} - \left(\frac{1}{Z_c(\gamma - 1)} + 1\right) \frac{p_0 w_0}{l\tilde{\rho}_0} \frac{\partial \tilde{\rho}_0}{\partial z} - \frac{\tilde{\rho}_0}{2P_c c_r h_0}\left(u_{s0}{}^3 f_{s0} + u_{r0}{}^3 f_{r0}\right) \tag{A39}$$

where,

$$u_{s0} = \sqrt{u_0{}^2 + w_0{}^2} \tag{A40}$$

$$u_{r0} = \sqrt{(u_0 - 1)^2 + w_0{}^2} \tag{A41}$$

$$f_{s0} = n_s\left(g\tilde{\rho}_0 h_0 u_{s0}\right)^{m_s} \tag{A42}$$

$$f_{r0} = n_r\left(g\tilde{\rho}_0 h_0 u_{r0}\right)^{m_r} \tag{A43}$$

$$g = \frac{2\rho_R \overline{C}_r R\omega}{\mu}. \tag{A44}$$

Matrix form of zeroth order perturbation governing equations are as follows:

Real Gas:

$$
\begin{bmatrix}
\tilde{\rho}_0 h_0 & 0 & 0 & w_0 h_0 \\
\dfrac{w_0}{l} & \dfrac{P_c}{l\tilde{\rho}_0} & 0 & 0 \\
0 & 0 & \dfrac{w_0}{l} & 0 \\
0 & \dfrac{\hat{u}_c \tilde{\rho}_0 w_0}{l}\dfrac{\partial \tilde{u}_0}{\partial p_0} & 0 & \dfrac{\hat{u}_c \tilde{\rho}_0 w_0}{l}\dfrac{\partial \tilde{u}_0}{\partial \tilde{\rho}_0} - \dfrac{p_0 w_0}{l\tilde{\rho}_0}
\end{bmatrix}
\begin{Bmatrix}
\dfrac{\partial w_0}{\partial z} \\
\dfrac{\partial p_0}{\partial z} \\
\dfrac{\partial u_0}{\partial z} \\
\dfrac{\partial \tilde{\rho}_0}{\partial z}
\end{Bmatrix}
=
\begin{Bmatrix}
-\tilde{\rho}_0 w_0 \dfrac{\partial h_0}{\partial z} \\
-\dfrac{w_0}{2c_r h_0}\left(u_{s0} f_{s0} + u_{r0} f_{r0}\right) \\
-\dfrac{1}{2c_r h_0}\left(u_0 u_{s0} f_{s0} + (u_0 - 1)u_{r0} f_{r0}\right) \\
\dfrac{\tilde{\rho}_0}{2P_c c_r h_0}\left(u_{s0}{}^3 f_{s0} + u_{r0}{}^3 f_{r0}\right)
\end{Bmatrix}
$$

$$(A45)$$

Ideal Gas:

$$
\begin{bmatrix}
\tilde{\rho}_0 h_0 & 0 & 0 & w_0 h_0 \\
\dfrac{w_0}{l} & \dfrac{P_c}{l\tilde{\rho}_0} & 0 & 0 \\
0 & 0 & \dfrac{w_0}{l} & 0 \\
0 & \dfrac{w_0}{lZ_c(\gamma - 1)} & 0 & -\dfrac{\left(1 + Z_c(\gamma - 1)\right)p_0 w_0}{lZ_c(\gamma - 1)\tilde{\rho}_0}
\end{bmatrix}
\begin{Bmatrix}
\dfrac{\partial w_0}{\partial z} \\
\dfrac{\partial p_0}{\partial z} \\
\dfrac{\partial u_0}{\partial z} \\
\dfrac{\partial \tilde{\rho}_0}{\partial z}
\end{Bmatrix}
=
\begin{Bmatrix}
-\tilde{\rho}_0 w_0 \dfrac{\partial h_0}{\partial z} \\
-\dfrac{w_0}{2c_r h_0}\left(u_{s0} f_{s0} + u_{r0} f_{r0}\right) \\
-\dfrac{1}{2c_r h_0}\left(u_0 u_{s0} f_{s0} + (u_0 - 1)u_{r0} f_{r0}\right) \\
\dfrac{\tilde{\rho}_0}{2P_c c_r h_0}\left(u_{s0}{}^3 f_{s0} + u_{r0}{}^3 f_{r0}\right)
\end{Bmatrix}
$$

$$(A46)$$

Zeroth order entrance and and exit conditions:

$$1 - p_0(0) = \frac{1+\xi}{2P_c}\tilde{\rho}_0(0)w_0{}^2(0) \tag{A47}$$

$$p_0(0) = \tilde{\rho}_0{}^{\gamma}(0) \tag{A48}$$

$$p_0(1) - p_S = -\frac{1-\xi_e}{2P_c}\tilde{\rho}_0(1)w_0{}^2(1) \tag{A49}$$

Non-dimensional mass-flow-rate is expressed with a production of non-dimensional density, axial velocity and local clearance.

$$\dot{\tilde{m}} = \frac{\dot{m}}{\pi D C_r R \omega \rho_R} = \tilde{\rho}_0 w_0 h_0 \tag{A50}$$

The zeroth order solution is solved iteratively by increasing $\dot{\tilde{m}}$ from very small value. If the calculated exit pressure is equal to sump pressure, or the calculated exit Mach number is equal to 1.0, whichever comes first, the iteration stops and the flow rate is saved. The case of exit Mach number being 1.0, is choked condition.

A.2.2 First Order Governing Equations

Continuity

$$0 = \tilde{\rho}_0 \frac{\partial h_1}{\partial \tau} + \left(h_0 + \gamma_c h_d\right) \frac{\partial \tilde{\rho}_1}{\partial \tau} + \tilde{\rho}_0 u_0 \frac{\partial h_1}{\partial \theta} + \tilde{\rho}_0 h_0 \frac{\partial u_1}{\partial \theta} + u_0 h_0 \frac{\partial \tilde{\rho}_1}{\partial \theta}$$
$$+ \frac{1}{l} \left[\frac{\partial \left(\tilde{\rho}_0 w_0 h_1 \right)}{\partial z} + \frac{\partial \left(\tilde{\rho}_0 w_1 h_0 \right)}{\partial z} + \frac{\partial \left(\tilde{\rho}_1 w_0 h_0 \right)}{\partial z} \right] \tag{A51}$$

Axial momentum

$$-\frac{P_c}{l \tilde{\rho}_0} \left(\frac{\partial p_1}{\partial z} - \frac{\tilde{\rho}_1}{\tilde{\rho}_0} \frac{\partial p_0}{\partial z} \right) = \frac{1}{2 c_r h_0} \left[w_0 u_{s0} \left(f_{s1} - \frac{h_1}{h_0} f_{s0} \right) + \left(w_1 u_{s0} + w_0 u_{s1} \right) f_{s0} \right]$$
$$+ \frac{1}{2 c_r h_0} \left[w_0 u_{r0} \left(f_{r1} - \frac{h_1}{h_0} f_{r0} \right) + \left(w_1 u_{r0} + w_0 u_{r1} \right) f_{r0} \right] \tag{A52}$$
$$+ \frac{\partial w_1}{\partial \tau} + u_0 \frac{\partial w_1}{\partial \theta} + \frac{1}{l} \left(w_0 \frac{\partial w_1}{\partial z} + w_1 \frac{\partial w_0}{\partial z} \right)$$

Circumferential momentum

$$-\frac{P_c}{\tilde{\rho}_0} \frac{\partial p_1}{\partial \theta} = \frac{1}{2 c_r h_0} \left[u_0 u_{s0} \left(f_{s1} - \frac{h_1}{h_0} f_{s0} \right) + \left(u_1 u_{s0} + u_0 u_{s1} \right) f_{s0} \right]$$
$$+ \frac{1}{2 c_r h_0} \left[(u_0 - 1) u_{r0} \left(f_{r1} - \frac{h_1}{h_0} f_{r0} \right) + \left(u_1 u_{r0} + (u_0 - 1) u_{r1} \right) f_{r0} \right] \tag{A53}$$
$$+ \frac{\partial u_1}{\partial \tau} + u_0 \frac{\partial u_1}{\partial \theta} + \frac{1}{l} \left(w_0 \frac{\partial u_1}{\partial z} + w_1 \frac{\partial u_0}{\partial z} \right)$$

Energy - Real Gas

$$\frac{p_0}{h_0}\frac{\partial h_1}{\partial \tau} = \hat{u}_c \tilde{\rho}_0 \left[\frac{\partial \tilde{\hat{u}}_1}{\partial p_1}\frac{\partial p_1}{\partial \tau} + u_0 \frac{\partial \tilde{\hat{u}}_1}{\partial p_1}\frac{\partial p_1}{\partial \theta} + \frac{1}{l}\left(w_0 \frac{\partial \tilde{\hat{u}}_1}{\partial p_1}\frac{\partial p_1}{\partial z} + w_1 \frac{\partial \tilde{\hat{u}}_0}{\partial p_0}\frac{\partial p_0}{\partial z} + \frac{\tilde{\rho}_1}{\tilde{\rho}_0} w_0 \frac{\partial \tilde{\hat{u}}_0}{\partial p_0}\frac{\partial p_0}{\partial z} \right) \right]$$

$$+ \hat{u}_c \tilde{\rho}_0 \left[\frac{\partial \tilde{\hat{u}}_1}{\partial \tilde{\rho}_1}\frac{\partial \tilde{\rho}_1}{\partial \tau} + u_0 \frac{\partial \tilde{\hat{u}}_1}{\partial \tilde{\rho}_1}\frac{\partial \tilde{\rho}_1}{\partial \theta} + \frac{1}{l}\left(w_0 \frac{\partial \tilde{\hat{u}}_1}{\partial \tilde{\rho}_1}\frac{\partial \tilde{\rho}_1}{\partial z} + w_1 \frac{\partial \tilde{\hat{u}}_0}{\partial \tilde{\rho}_0}\frac{\partial \tilde{\rho}_0}{\partial z} + \frac{\tilde{\rho}_1}{\tilde{\rho}_0} w_0 \frac{\partial \tilde{\hat{u}}_0}{\partial \tilde{\rho}_0}\frac{\partial \tilde{\rho}_0}{\partial z} \right) \right]$$

$$- \frac{p_0}{\tilde{\rho}_0} \left[\frac{\partial \tilde{\rho}_1}{\partial \tau} + u_0 \frac{\partial \tilde{\rho}_1}{\partial \theta} + \frac{1}{l}\left(w_0 \frac{\partial \tilde{\rho}_1}{\partial z} + w_1 \frac{\partial \tilde{\rho}_0}{\partial z} + \frac{p_1}{p_0} w_0 \frac{\partial \tilde{\rho}_0}{\partial z} - \frac{\tilde{\rho}_1}{\tilde{\rho}_0} w_0 \frac{\partial \tilde{\rho}_0}{\partial z} \right) \right]$$

$$+ \frac{\gamma_c h_d}{h_0} \left[\hat{u}_c \tilde{\rho}_0 \frac{\partial \tilde{\hat{u}}_1}{\partial p_1}\frac{\partial p_1}{\partial \tau} + \left(\hat{u}_c \tilde{\rho}_0 \frac{\partial \tilde{\hat{u}}_1}{\partial \tilde{\rho}_1} - \frac{p_0}{\tilde{\rho}_0} \right)\frac{\partial \tilde{\rho}_1}{\partial \tau} + \frac{\tilde{\rho}_0}{P_c}\left(u_0 \frac{\partial u_1}{\partial \tau} + w_0 \frac{\partial w_1}{\partial \tau} \right) \right]$$

$$- \frac{\tilde{\rho}_0}{2 P_c c_r h_0} \left[u_{s0}{}^2 \left(u_{s0} f_{s1} + 3 u_{s1} f_{s0} \right) + \left(\frac{\tilde{\rho}_1}{\tilde{\rho}_0} - \frac{h_1}{h_0} \right) u_{s0}{}^3 f_{s0} \right]$$

$$- \frac{\tilde{\rho}_0}{2 P_c c_r h_0} \left[u_{r0}{}^2 \left(u_{r0} f_{r1} + 3 u_{r1} f_{r0} \right) + \left(\frac{\tilde{\rho}_1}{\tilde{\rho}_0} - \frac{h_1}{h_0} \right) u_{r0}{}^3 f_{r0} \right]$$

(A54)

where,

$$\tilde{\hat{u}}_1 = \frac{\partial \tilde{\hat{u}}_0(p_0, \tilde{\rho}_0)}{\partial p_0} p_1 + \frac{\partial \tilde{\hat{u}}_0(p_0, \tilde{\rho}_0)}{\partial \tilde{\rho}_0} \tilde{\rho}_1 . \tag{A55}$$

Substituting (A55) into (A54) yields,

$$\frac{p_0}{h_0}\frac{\partial h_1}{\partial \tau} = \hat{u}_c \tilde{\rho}_0 \frac{\partial \tilde{\tilde{u}}_0}{\partial p_0}\left[\frac{\partial p_1}{\partial \tau} + u_0 \frac{\partial p_1}{\partial \theta} + \frac{1}{l}\left(w_0 \frac{\partial p_1}{\partial z} + w_1 \frac{\partial p_0}{\partial z} + \frac{\tilde{\rho}_1}{\tilde{\rho}_0} w_0 \frac{\partial p_0}{\partial z}\right)\right]$$

$$+\hat{u}_c \tilde{\rho}_0 \frac{\partial \tilde{\tilde{u}}_0}{\partial \tilde{\rho}_0}\left[\frac{\partial \tilde{\rho}_1}{\partial \tau} + u_0 \frac{\partial \tilde{\rho}_1}{\partial \theta} + \frac{1}{l}\left(w_0 \frac{\partial \tilde{\rho}_1}{\partial z} + w_1 \frac{\partial \tilde{\rho}_0}{\partial z} + \frac{\tilde{\rho}_1}{\tilde{\rho}_0} w_0 \frac{\partial \tilde{\rho}_0}{\partial z}\right)\right]$$

$$-\frac{p_0}{\tilde{\rho}_0}\left[\frac{\partial \tilde{\rho}_1}{\partial \tau} + u_0 \frac{\partial \tilde{\rho}_1}{\partial \theta} + \frac{1}{l}\left(w_0 \frac{\partial \tilde{\rho}_1}{\partial z} + w_1 \frac{\partial \tilde{\rho}_0}{\partial z} + \frac{p_1}{p_0} w_0 \frac{\partial \tilde{\rho}_0}{\partial z} - \frac{\tilde{\rho}_1}{\tilde{\rho}_0} w_0 \frac{\partial \tilde{\rho}_0}{\partial z}\right)\right]$$

$$+\frac{\gamma_c h_d}{h_0}\left[\hat{u}_c \tilde{\rho}_0 \frac{\partial \tilde{\tilde{u}}_0}{\partial p_0}\frac{\partial p_1}{\partial \tau} + \left(\hat{u}_c \tilde{\rho}_0 \frac{\partial \tilde{\tilde{u}}_0}{\partial \tilde{\rho}_0} - \frac{p_0}{\tilde{\rho}_0}\right)\frac{\partial \tilde{\rho}_1}{\partial \tau} + \frac{\tilde{\rho}_0}{P_c}\left(u_0 \frac{\partial u_1}{\partial \tau} + w_0 \frac{\partial w_1}{\partial \tau}\right)\right]$$

$$-\frac{\tilde{\rho}_0}{2P_c c_r h_0}\left[u_{s0}{}^2 \left(u_{s0} f_{s1} + 3u_{s1} f_{s0}\right) + \left(\frac{\tilde{\rho}_1}{\tilde{\rho}_0} - \frac{h_1}{h_0}\right)u_{s0}{}^3 f_{s0}\right]$$

$$-\frac{\tilde{\rho}_0}{2P_c c_r h_0}\left[u_{r0}{}^2 \left(u_{r0} f_{r1} + 3u_{r1} f_{r0}\right) + \left(\frac{\tilde{\rho}_1}{\tilde{\rho}_0} - \frac{h_1}{h_0}\right)u_{r0}{}^3 f_{r0}\right]$$

$$\tag{A56}$$

Energy - Ideal Gas

$$\frac{p_0}{h_0}\frac{\partial h_1}{\partial \tau} = \frac{1}{Z_c(\gamma-1)}\left[\frac{\partial p_1}{\partial \tau} + u_0 \frac{\partial p_1}{\partial \theta} + \frac{1}{l}\left(w_0 \frac{\partial p_1}{\partial z} + w_1 \frac{\partial p_0}{\partial z}\right)\right]$$

$$-\left(\frac{1}{Z_c(\gamma-1)} + 1\right)\frac{p_0}{\tilde{\rho}_0}\left[\frac{\partial \tilde{\rho}_1}{\partial \tau} + u_0 \frac{\partial \tilde{\rho}_1}{\partial \theta} + \frac{1}{l}\left(w_0 \frac{\partial \tilde{\rho}_1}{\partial z} + w_1 \frac{\partial \tilde{\rho}_0}{\partial z} + \frac{p_1}{p_0} w_0 \frac{\partial \tilde{\rho}_0}{\partial z} - \frac{\tilde{\rho}_1}{\tilde{\rho}_0} w_0 \frac{\partial \tilde{\rho}_0}{\partial z}\right)\right]$$

$$+\frac{\gamma_c h_d}{h_0}\left[\frac{1}{Z_c(\gamma-1)}\frac{\partial p_1}{\partial \tau} - \left(\frac{1}{Z_c(\gamma-1)} + 1\right)\frac{p_0}{\tilde{\rho}_0}\frac{\partial \tilde{\rho}_1}{\partial \tau} + \frac{\tilde{\rho}_0}{P_c}\left(u_0 \frac{\partial u_1}{\partial \tau} + w_0 \frac{\partial w_1}{\partial \tau}\right)\right]$$

$$-\frac{\tilde{\rho}_0}{2P_c c_r h_0}\left[u_{s0}{}^2 \left(u_{s0} f_{s1} + 3u_{s1} f_{s0}\right) + \left(\frac{\tilde{\rho}_1}{\tilde{\rho}_0} - \frac{h_1}{h_0}\right)u_{s0}{}^3 f_{s0}\right]$$

$$-\frac{\tilde{\rho}_0}{2P_c c_r h_0}\left[u_{r0}{}^2 \left(u_{r0} f_{r1} + 3u_{r1} f_{r0}\right) + \left(\frac{\tilde{\rho}_1}{\tilde{\rho}_0} - \frac{h_1}{h_0}\right)u_{r0}{}^3 f_{r0}\right]$$

$$\tag{A57}$$

where,

$$u_{s1} = \frac{u_0 u_1 + w_0 w_1}{u_{s0}} \tag{A58}$$

$$u_{r1} = \frac{(u_0 - 1)u_1 + w_0 w_1}{u_{r0}} \tag{A59}$$

and,

$$f_{s1} = m_s f_{s0} \left(\frac{\tilde{\rho}_1}{\tilde{\rho}_0} + \frac{h_1}{h_0} + \frac{u_{s1}}{u_{s0}} \right) \tag{A60}$$

$$f_{r1} = m_r f_{r0} \left(\frac{\tilde{\rho}_1}{\tilde{\rho}_0} + \frac{h_1}{h_0} + \frac{u_{r1}}{u_{r0}} \right). \tag{A61}$$

Clearance function with tilting motion of rotor is,

$$h = h_0 - \left[x + \alpha_Y \left(\frac{L}{C_r} \right) (z - z_0) \right] \cos\theta - \left[y - \alpha_X \left(\frac{L}{C_r} \right) (z - z_0) \right] \sin\theta. \tag{A62}$$

Comparing to (A29),

$$\varepsilon h_1 = - \left[x + \alpha_Y \left(\frac{L}{C_r} \right) (z - z_0) \right] \cos\theta - \left[y - \alpha_X \left(\frac{L}{C_r} \right) (z - z_0) \right] \sin\theta. \tag{A63}$$

Assuming the dependent perturbation variables as,

$$w_1(z,\tau,\theta) = w_{1c}(z,\tau)\cos\theta + w_{1s}(z,\tau)\sin\theta \tag{A64}$$

$$p_1(z,\tau,\theta) = p_{1c}(z,\tau)\cos\theta + p_{1s}(z,\tau)\sin\theta \tag{A65}$$

$$u_1(z,\tau,\theta) = u_{1c}(z,\tau)\cos\theta + u_{1s}(z,\tau)\sin\theta \tag{A66}$$

$$\tilde{\rho}_1(z,\tau,\theta) = \tilde{\rho}_{1c}(z,\tau)\cos\theta + \tilde{\rho}_{1s}(z,\tau)\sin\theta. \tag{A67}$$

Complex variables are introduced as following:

$$\boldsymbol{w}_1 = w_{1c} + jw_{1s} \tag{A68}$$

$$\boldsymbol{p}_1 = p_{1c} + jp_{1s} \tag{A69}$$

$$\boldsymbol{u}_1 = u_{1c} + ju_{1s} \tag{A70}$$

$$\tilde{\boldsymbol{\rho}}_1 = \tilde{\rho}_{1c} + j\rho_{1s} \tag{A71}$$

$$\varepsilon \boldsymbol{h}_1 = -(\boldsymbol{r} + \boldsymbol{\alpha}) \tag{A72}$$

$$\boldsymbol{r} = x + jy \tag{A73}$$

$$\boldsymbol{\alpha} = \alpha_Y - j\alpha_X. \tag{A74}$$

Assumimg a pressional seal motion of the form, the displacement motion and tilting motion are expressed as,

$$r = r_0 e^{jf\tau} \tag{A75}$$

$$\alpha = \alpha_0 e^{jf\tau} \tag{A76}$$

$$h_1 = h_{10} e^{jf\tau} \tag{A77}$$

where,

$$f = \frac{\Omega}{\omega}. \tag{A78}$$

Introducing the following complex variables:

$$w_1 = w_1 e^{jf\tau} \tag{A79}$$

$$p_1 = p_1 e^{jf\tau} \tag{A80}$$

$$u_1 = u_1 e^{jf\tau} \tag{A81}$$

$$\tilde{\rho}_1 = \tilde{\rho}_1 e^{jf\tau}. \tag{A82}$$

The first order governing equations are expressed in matrix form.

$$[A(z)]\frac{d}{dz}\begin{Bmatrix} w_1 \\ p_1 \\ u_1 \\ \tilde{\rho}_1 \end{Bmatrix} + [B(z,f)]\begin{Bmatrix} w_1 \\ p_1 \\ u_1 \\ \tilde{\rho}_1 \end{Bmatrix} = \frac{r_0}{\varepsilon}\begin{Bmatrix} g_1(z,f) \\ g_2(z,f) \\ g_3(z,f) \\ g_4(z,f) \end{Bmatrix} + \frac{\alpha_0}{\varepsilon}\frac{L}{C_r}\begin{Bmatrix} g_5(z,f) \\ g_6(z,f) \\ g_7(z,f) \\ g_8(z,f) \end{Bmatrix} \tag{A83}$$

The components of matrix A, B and vector g are given in the Appendix B.

There are four boundary conditions for first order perturbation governing equations. The first one states that circumferential velocity at the inlet does not perturb.

$$u_1(0) = 0 \tag{A84}$$

The second and third boundary conditions come from inlet pressure loss model and isentropic relationship between pressure and density at the inlet.

$$p_1(0) = -\frac{1+\xi}{2}\frac{1}{P_c}\left(\tilde{\rho}_1(0)w_0^2(0) + 2\tilde{\rho}_0(0)w_0(0)w_1(0)\right) \tag{A85}$$

$$p_1(0) = r\tilde{\rho}_1(0)\tilde{\rho}_0^{\gamma-1}(0) \tag{A86}$$

The last one is presented for each case of choked and unchoked condition. For unchoked situation, the exit pressure recovery model is presented for exit boundary condition.

$$p_1(1) = -\frac{1-\xi_e}{2}\frac{1}{P_c}\left(\tilde{\rho}_1(1)w_0{}^2(1) + 2\tilde{\rho}_0(1)w_0(1)w_1(1)\right) \tag{A87}$$

In case the flow is choked at the exit, Mach number will not perturb at the exit.

$$Ma_1(1) = 0 \tag{A88}$$

using the ideal gas mach number,

$$Ma = W\sqrt{\frac{\rho}{\gamma P}} = w\sqrt{\frac{\tilde{\rho}}{\gamma P_c p}}\ . \tag{A89}$$

The zeroth and first perturbation version of Mach is,

$$Ma_0 = w_0\sqrt{\frac{\tilde{\rho}_0}{\gamma P_c p_0}}\ , \tag{A90}$$

$$Ma_1 = Ma_0\left(\frac{\tilde{\rho}_1}{2\tilde{\rho}_0} + \frac{w_1}{w_0} - \frac{p_1}{2p_0}\right). \tag{A91}$$

These yield the last boundary condition for choked condition.

$$\frac{\tilde{\rho}_1(1)}{2\tilde{\rho}_0(1)} + \frac{w_1(1)}{w_0(1)} - \frac{p_1(1)}{2p_0(1)} = 0 \tag{A92}$$

The missing boundary conditions are found by transition matrix approach, Childs [12]. Once frequency dependent first order perturbation solutions are found, non-dimensional reaction force and moment components for each frequency are obtained by integrating first order pressure through the whole seal length.

$$\tilde{F}_X = -\pi\int_0^1 \text{Re}[p_1(f)]dz \tag{A93}$$

$$\tilde{F}_Y = -\pi\int_0^1 \text{Im}[p_1(f)]dz \tag{A94}$$

$$\tilde{M}_Y = \pi\int_0^1 \text{Re}[p_1(f)](z-z_0)dz \tag{A95}$$

$$\tilde{M}_X = -\pi\int_0^1 \text{Im}[p_1(f)](z-z_0)dz \tag{A96}$$

To get frequency dependent 4×4 full rotordynamic coefficients, force and moment of (A93)-(A96) are calculated for displacement motion without tilting ($\frac{\alpha_0}{\varepsilon} = 0$), and tilting motion with no displacement ($\frac{r_0}{\varepsilon} = 0$). Now dimensional force and moment components are found as following:

$$F_X = \frac{P_R L D}{2 C_r} \tilde{F}_X \tag{A97}$$

$$F_Y = \frac{P_R L D}{2 C_r} \tilde{F}_Y \tag{A98}$$

$$M_X = \frac{P_R L^2 D}{2 C_r} \tilde{M}_X \tag{A99}$$

$$M_Y = \frac{P_R L^2 D}{2 C_r} \tilde{M}_Y \tag{A100}$$

The general transfer function on two-control-volume is,

$$-\begin{Bmatrix} F_X(j\Omega) \\ F_Y(j\Omega) \\ M_Y(j\Omega) \\ M_X(j\Omega) \end{Bmatrix} = \begin{bmatrix} D(j\Omega) & E(j\Omega) & D_{\varepsilon\alpha}(j\Omega) & -E_{\varepsilon\alpha}(j\Omega) \\ -E(j\Omega) & D(j\Omega) & -E_{\varepsilon\alpha}(j\Omega) & -D_{\varepsilon\alpha}(j\Omega) \\ D_{\alpha\varepsilon}(j\Omega) & E_{\alpha\varepsilon}(j\Omega) & D_\alpha(j\Omega) & -E_\alpha(j\Omega) \\ E_{\alpha\varepsilon}(j\Omega) & -D_{\alpha\varepsilon}(j\Omega) & E_\alpha(j\Omega) & D_\alpha(j\Omega) \end{bmatrix} \begin{Bmatrix} X(j\Omega) \\ Y(j\Omega) \\ \alpha_Y(j\Omega) \\ \alpha_X(j\Omega) \end{Bmatrix}$$

$$\tag{A101}$$

where,

$$D(j\Omega) = K(\Omega) + jC(\Omega) \tag{A102}$$

$$E(j\Omega) = k(\Omega) + jc(\Omega) \tag{A103}$$

$$D_{\varepsilon\alpha}(j\Omega) = K_{\varepsilon\alpha}(\Omega) + jC_{\varepsilon\alpha}(\Omega) \tag{A104}$$

$$E_{\varepsilon\alpha}(j\Omega) = k_{\varepsilon\alpha}(\Omega) + jc_{\varepsilon\alpha}(\Omega) \tag{A105}$$

$$D_{\alpha\varepsilon}(j\Omega) = K_{\alpha\varepsilon}(\Omega) + jC_{\alpha\varepsilon}(\Omega) \tag{A106}$$

$$E_{\alpha\varepsilon}(j\Omega) = k_{\alpha\varepsilon}(\Omega) + jc_{\alpha\varepsilon}(\Omega) \tag{A107}$$

$$D_\alpha(j\Omega) = K_\alpha(\Omega) + jC_\alpha(\Omega) \tag{A108}$$

$$E_\alpha(j\Omega) = k_\alpha(\Omega) + jc_\alpha(\Omega) \tag{A109}$$

In terms of frequency dependent rotordynamic coefficients, the model is,

$$
-\begin{Bmatrix} \boldsymbol{F}_X \\ \boldsymbol{F}_Y \\ \boldsymbol{M}_Y \\ \boldsymbol{M}_X \end{Bmatrix} = \begin{bmatrix} K(\Omega) & k(\Omega) & K_{\varepsilon\alpha}(\Omega) & -k_{\varepsilon\alpha}(\Omega) \\ -k(\Omega) & K(\Omega) & -k_{\varepsilon\alpha}(\Omega) & -K_{\varepsilon\alpha}(\Omega) \\ K_{\alpha\varepsilon}(\Omega) & k_{\alpha\varepsilon}(\Omega) & K_\alpha(\Omega) & -k_\alpha(\Omega) \\ k_{\alpha\varepsilon}(\Omega) & -K_{\alpha\varepsilon}(\Omega) & k_\alpha(\Omega) & K_\alpha(\Omega) \end{bmatrix} \begin{Bmatrix} X \\ Y \\ \alpha_Y \\ \alpha_X \end{Bmatrix}
$$
$$
+ \begin{bmatrix} C(\Omega) & c(\Omega) & C_{\varepsilon\alpha}(\Omega) & -c_{\varepsilon\alpha}(\Omega) \\ -c(\Omega) & C(\Omega) & -c_{\varepsilon\alpha}(\Omega) & -C_{\varepsilon\alpha}(\Omega) \\ C_{\alpha\varepsilon}(\Omega) & c_{\alpha\varepsilon}(\Omega) & C_\alpha(\Omega) & -c_\alpha(\Omega) \\ c_{\alpha\varepsilon}(\Omega) & -C_{\alpha\varepsilon}(\Omega) & c_\alpha(\Omega) & C_\alpha(\Omega) \end{bmatrix} \begin{Bmatrix} \dot{X} \\ \dot{Y} \\ \dot{\alpha}_Y \\ \dot{\alpha}_X \end{Bmatrix}
$$

(A110)

APPENDIX B

MATRIX AND VECTOR ELEMENTS FOR FIRST ORDER SOLUTION

B.1 Real Gas

Matrix A

$$A_{11} = \frac{\tilde{\rho}_0 h_0}{l} \tag{B1}$$

$$A_{12} = 0 \tag{B2}$$

$$A_{13} = 0 \tag{B3}$$

$$A_{14} = \frac{w_0 h_0}{l} \tag{B4}$$

$$A_{21} = \frac{w_0}{l} \tag{B5}$$

$$A_{22} = \frac{P_c}{l \tilde{\rho}_0} \tag{B6}$$

$$A_{23} = 0 \tag{B7}$$

$$A_{24} = 0 \tag{B8}$$

$$A_{31} = 0 \tag{B9}$$

$$A_{32} = 0 \tag{B10}$$

$$A_{33} = \frac{w_0}{l} \tag{B11}$$

$$A_{34} = 0 \tag{B12}$$

$$A_{41} = 0 \tag{B13}$$

$$A_{42} = \hat{u}_c \frac{\partial \tilde{\tilde{u}}_0}{\partial p_0} \frac{\tilde{\rho}_0 w_0}{l} \tag{B14}$$

$$A_{43} = 0 \tag{B15}$$

$$A_{44} = \hat{u}_c \frac{\partial \tilde{\tilde{u}}_0}{\partial \tilde{\rho}_0} \frac{\tilde{\rho}_0 w_0}{l} - \frac{p_0 w_0}{l \tilde{\rho}_0} \tag{B16}$$

Matrix **B**

$$B_{11} = \frac{\tilde{\rho}_0}{l}\frac{\partial h_0}{\partial z} + \frac{h_0}{l}\frac{\partial \tilde{\rho}_0}{\partial z} \tag{B17}$$

$$B_{12} = 0 \tag{B18}$$

$$B_{13} = j\left[-\tilde{\rho}_0 h_0\right] \tag{B19}$$

$$B_{14} = \frac{w_0}{l}\frac{\partial h_0}{\partial z} + \frac{h_0}{l}\frac{\partial w_0}{\partial z} + j\left[f\left(h_0 + \gamma_c h_d\right) - u_0 h_0\right] \tag{B20}$$

$$B_{21} = \frac{1}{l}\frac{\partial w_0}{\partial z} + \frac{w_0^2}{2c_r h_0}\left(\frac{(m_s+1)f_{s0}}{u_{s0}} + \frac{(m_r+1)f_{r0}}{u_{r0}}\right) + \frac{1}{2c_r h_0}\left(u_{s0}f_{s0} + u_{r0}f_{r0}\right) + j\left[f - u_0\right]$$
$$\tag{B21}$$

$$B_{22} = 0 \tag{B22}$$

$$B_{23} = \frac{w_0}{2c_r h_0}\left(\frac{(m_s+1)u_0 f_{s0}}{u_{s0}} + \frac{(m_r+1)(u_0-1)f_{r0}}{u_{r0}}\right) \tag{B23}$$

$$B_{24} = -\frac{P_c}{l\tilde{\rho}_0^2}\frac{\partial p_0}{\partial z} + \frac{w_0}{2c_r h_0 \tilde{\rho}_0}\left(m_s u_{s0} f_{s0} + m_r u_{r0} f_{r0}\right) \tag{B24}$$

$$B_{31} = \frac{1}{l}\frac{\partial u_0}{\partial z} + \frac{w_0}{2c_r h_0}\left(\frac{(m_s+1)u_0 f_{s0}}{u_{s0}} + \frac{(m_r+1)(u_0-1)f_{r0}}{u_{r0}}\right) \tag{B25}$$

$$B_{32} = j\left[-\frac{P_c}{\tilde{\rho}_0}\right] \tag{B26}$$

$$B_{33} = \frac{1}{2c_r h_0}\left(\frac{(m_s+1)u_0^2 f_{s0}}{u_{s0}} + \frac{(m_r+1)(u_0-1)^2 f_{r0}}{u_{r0}}\right) + \frac{1}{2c_r h_0}\left(u_{s0}f_{s0} + u_{r0}f_{r0}\right) + j\left[f - u_0\right]$$
$$\tag{B27}$$

$$B_{34} = \frac{1}{2c_r h_0 \tilde{\rho}_0}\left(m_s u_0 u_{s0} f_{s0} + m_r (u_0-1)u_{r0} f_{r0}\right) \tag{B28}$$

$$B_{41} = \frac{\hat{u}_c \tilde{\rho}_0}{l} \left(\frac{\partial \tilde{\tilde{u}}_0}{\partial p_0} \frac{\partial p_0}{\partial z} + \frac{\partial \tilde{\tilde{u}}_0}{\partial \tilde{\rho}_0} \frac{\partial \tilde{\rho}_0}{\partial z} \right) - \frac{p_0}{l \tilde{\rho}_0} \frac{\partial \tilde{\rho}_0}{\partial z} - \frac{\tilde{\rho}_0 w_0}{2 P_c c_r h_0} \left((m_s + 3) u_{s0} f_{s0} + (m_r + 3) u_{r0} f_{r0} \right)$$
$$+ j \left[f \frac{\gamma_c h_d \tilde{\rho}_0 w_0}{P_c h_0} \right]$$

(B29)

$$B_{42} = -\frac{w_0}{l \tilde{\rho}_0} \frac{\partial \tilde{\rho}_0}{\partial z} + j \left[f \hat{u}_c \frac{\partial \tilde{\tilde{u}}_0}{\partial p_0} \tilde{\rho}_0 \left(1 + \frac{\gamma_c h_d}{h_0} \right) - \hat{u}_c \frac{\partial \tilde{\tilde{u}}_0}{\partial p_0} \tilde{\rho}_0 u_0 \right]$$ (B30)

$$B_{43} = -\frac{\tilde{\rho}_0}{2 P_c c_r h_0} \left((m_s + 3) u_0 u_{s0} f_{s0} + (m_r + 3)(u_0 - 1) u_{r0} f_{r0} \right) + j \left[f \frac{\gamma_c h_d \tilde{\rho}_0 u_0}{P_c h_0} \right]$$ (B31)

$$B_{44} = \frac{\hat{u}_c w_0}{l} \left(\frac{\partial \tilde{\tilde{u}}_0}{\partial p_0} \frac{\partial p_0}{\partial z} + \frac{\partial \tilde{\tilde{u}}_0}{\partial \tilde{\rho}_0} \frac{\partial \tilde{\rho}_0}{\partial z} \right) + \frac{p_0 w_0}{l \tilde{\rho}_0^2} \frac{\partial \tilde{\rho}_0}{\partial z} - \frac{1}{2 P_c c_r h_0} \left((m_s + 1) u_{s0}^3 f_{s0} + (m_r + 1) u_{r0}^3 f_{r0} \right)$$
$$+ j \left[f \left(\hat{u}_c \tilde{\rho}_0 \frac{\partial \tilde{\tilde{u}}_0}{\partial \tilde{\rho}_0} - \frac{p_0}{\tilde{\rho}_0} \right) \left(1 + \frac{\gamma_c h_d}{h_0} \right) - \hat{u}_c \tilde{\rho}_0 u_0 \frac{\partial \tilde{\tilde{u}}_0}{\partial \tilde{\rho}_0} + \frac{p_0 u_0}{\tilde{\rho}_0} \right]$$

(B32)

Vector $\boldsymbol{g}$

$$g_1 = \frac{\tilde{\rho}_0}{l} \frac{\partial w_0}{\partial z} + \frac{w_0}{l} \frac{\partial \tilde{\rho}_0}{\partial z} + j \left[f \tilde{\rho}_0 - \tilde{\rho}_0 u_0 \right]$$ (B33)

$$g_2 = \frac{w_0}{2 c_r h_0^2} \left((m_s - 1) u_{s0} f_{s0} + (m_r - 1) u_{r0} f_{r0} \right)$$ (B34)

$$g_3 = \frac{1}{2 c_r h_0^2} \left((m_s - 1) u_0 u_{s0} f_{s0} + (m_r - 1)(u_0 - 1) u_{r0} f_{r0} \right)$$ (B35)

$$g_4 = -\frac{\tilde{\rho}_0}{2 P_c c_r h_0^2} \left((m_s - 1) u_{s0}^3 f_{s0} + (m_r - 1) u_{r0}^3 f_{r0} \right) + j \left[-f \frac{p_0}{h_0} \right]$$ (B36)

$$g_5 = \frac{\tilde{\rho}_0 w_0}{l} + g_1 (z - z_0)$$ (B37)

$$g_6 = g_2 (z - z_0)$$ (B38)

$$g_7 = g_3 \left(z - z_0 \right) \tag{B39}$$

$$g_8 = g_4 \left(z - z_0 \right) \tag{B40}$$

B.2 Ideal Gas

The rest of components other than those given here are not changed.

$$A_{42} = \frac{w_0}{lZ_c(\gamma - 1)} \tag{B41}$$

$$A_{44} = -\frac{\left(1 + Z_c(\gamma - 1)\right) p_0 w_0}{lZ_c(\gamma - 1)\tilde{\rho}_0} \tag{B42}$$

$$B_{41} = \frac{1}{lZ_c(\gamma - 1)} \frac{\partial p_0}{\partial z} - \frac{\left(1 + Z_c(\gamma - 1)\right) p_0}{lZ_c(\gamma - 1)\tilde{\rho}_0} \frac{\partial \tilde{\rho}_0}{\partial z} - \frac{\tilde{\rho}_0 w_0}{2 P_c c_r h_0} \left((m_s + 3) u_{s0} f_{s0} + (m_r + 3) u_{r0} f_{r0} \right)$$
$$+ j \left[f \frac{\gamma_c h_d \tilde{\rho}_0 w_0}{P_c h_0} \right]$$
$$\tag{B43}$$

$$B_{42} = -\frac{\left(1 + Z_c(\gamma - 1)\right) w_0}{lZ_c(\gamma - 1)\tilde{\rho}_0} \frac{\partial \tilde{\rho}_0}{\partial z} + j \left[f \frac{h_0 + \gamma_c h_d}{Z_c(\gamma - 1)h_0} - \frac{u_0}{Z_c(\gamma - 1)} \right] \tag{B44}$$

$$B_{44} = \frac{\left(1 + Z_c(\gamma - 1)\right) p_0 w_0}{lZ_c(\gamma - 1)\tilde{\rho}_0^2} \frac{\partial \tilde{\rho}_0}{\partial z} - \frac{1}{2 P_c c_r h_0} \left((m_s + 1) u_{s0}^3 f_{s0} + (m_r + 1) u_{r0}^3 f_{r0} \right)$$
$$+ j \left[-f \frac{\left(1 + Z_c(\gamma - 1)\right)\left(h_0 + \gamma_c h_d\right) p_0}{Z_c(\gamma - 1)h_0 \tilde{\rho}_0} + \frac{\left(1 + Z_c(\gamma - 1)\right) p_0 u_0}{Z_c(\gamma - 1)\tilde{\rho}_0} \right]$$
$$\tag{B45}$$

VITA

Name: Yoon Shik Shin

Address: 670 Daechi 1-dong Kangnam-ku, Dongbu Centreville Apt. 102-1201,
                Seoul 135-838, Republic of Korea

Email Address: yoonshik@gmail.com

Education: B.S., Mechanical Engineering, Yonsei University, 2002
                M.S., Mechanical Engineering, Texas A&M University, 2005